11-2013

Nonlinear Energy Harvesting Under White Noise

Qifan He
Clemson University, qifanh@g.clemson.edu

Nonlinear Energy Harvesting Under White Noise

A Dissertation
Presented to
the Graduate School of
Clemson University

In Partial Fulfillment
of the Requirements for the Degree
Master of Science
Mechanical Engineering

---

by
Qifan He
November 2013

Accepted by:
Dr. Mohammed Daqaq, Committee Chair
Dr. Ardalan Vahidi
Dr. Georges Fadel

Abstract

While purposeful introduction of stiffness nonlinearities into the dynamics of energy harvesters is aimed at enhancing performance under non-stationary and random excitations, most of the conclusions reported in the current literature are based on the steady-state response which assumes a harmonic fixed-frequency excitation. As a result, we still do not have a clear understanding of how the nature of the excitation influences the output power, or what role stiffness nonlinearities play in the transduction of energy harvesters under random excitations.

To fill this gap in the current knowledge, this thesis investigates the response of nonlinear mono- and bi-stable energy harvesters to environmental excitations that can be approximated via a white noise process. For the mono-stable case, statistical linearization is utilized to analytically approximate the statistical averages of the response. The influence of the nonlinearity and the symmetry of the restoring force on the mean power is investigated under optimal electric loading conditions. It is shown that the nonlinearity has no influence on the output power unless the ratio between the time constant of the harvesting circuit and the period of the mechanical oscillator is small. In such case, a mono-stable harvester with a symmetric nonlinear restoring force can never produce higher mean power levels than an equivalent linear harvester regardless of the magnitude or nature of the nonlinearity. On the other hand, asymmetries in the restoring force are shown to provide performance improvements over an equivalent linear harvester.

For energy harvesters with a bi-stable potential function, statistical linearization, direct numerical integration of the stochastic differential equations, and finite element solu-

tion of the Fokker-Plank-Kolmogorov equation governing the response probability density function are utilized to understand how the shape and symmetry of the potential energy function influence the mean output power of the harvester. It is observed that, both of the finite element solution and the direct numerical integration provide close predictions for the mean power regardless of the shape of the potential energy function. Statistical linearization, on the other hand, yields non-unique and erroneous predictions unless the potential energy function has shallow potential wells. It is shown that the mean power exhibits a maximum value at an optimal potential shape. This optimal shape is not directly related to the shape that maximizes the mean square displacement even when the time constant ratio, i.e., ratio between the time constants of the mechanical and electrical systems is small. Maximizing the mean square displacement yields a potential shape with a global maximum (unstable potential) for any value of the time constant ratio and any noise intensity, whereas maximizing the average power yields a bi-stable potential which possesses deeper potential wells for larger noise intensities and vise versa. Away from the optimal shape, the mean power drops significantly highlighting the importance of characterizing the noise intensity of the vibration source prior to designing a bi-stable harvester for the purpose of harnessing energy from white noise excitations. Furthermore, it is demonstrated that, the optimal time constant ratio is not necessarily small which challenges previous conceptions that a bi-stable harvester provides better output power when the time constant ratio is small. While maximum variation of the mean power with the nonlinearity occurs for smaller values of the time constant ratio, these values do not necessarily correspond to the optimal performance of the harvester. Finally, it is shown that asymmetries in the potential shape of bi-stable harvesters do not improve the mean power unless the symmetric potential function is designed away from its optimal parameters.

Dedication

I would like to dedicate this thesis to my parents for all the love and support.

Acknowledgments

First and foremost, I would like to thank my advisor Dr. Mohammed F. Daqaq, for his invaluable guidance and distinguished support. Without his insightful supervision and persistent help, the completion of my master's work would have not been possible. It is my great honor to have him as my advisor as well as a friend, who offered me the freedom to conduct my research independently and provided valuable suggestions whenever it was needed. I thank him for his complete trust, remarkable comments and patient guidance.

I would also like to thank my committee members, Drs. Ardalan Vahidi and Georges Fadel for devoting their time to review my thesis. Their encouragement and feedback are helpful throughout the process. My deep appreciation and sincere gratitude go to Dr. Gang Li, for providing valuable guidance towards the completion of this thesis.

I acknowledge the financial support from the National Science Foundation for providing the invaluable opportunity to conduct this research. I would also like to express my great appreciation to the members of the Nonlinear Vibrations and Energy Harvesting Laboratory (NOVEHL); in particular, Dr. Ravindra Masana, Mr. Amin Bibo, Mr. Shyam Panyam, Mr. Clodoaldo Silva, Mr. Saad Alazemi, Mr. Rajendran Raveen, Mr. Ali Alhadidi, and Mr. Cheng Luo.

Finally, I would like to thank my friends with whom I have studied, worked, and played in the Department of Mechanical Engineering in Clemson.

Table of Contents

List of Figures

Chapter 1

Introduction

Energy harvesting is the process by which ambient energy is captured and transformed into a useful form. Historically, mankind has relied on this process to fill its basic energy needs using windmills, sailing ships, and waterwheels. However, our ever increasing energy demands and changing research trends is pushing these old concepts into newer directions. For instance, today, we continue to produce smaller and lower-power consumption devices that span different fields of technology. Wireless sensors, data transmitters, controllers, and implantable medical devices that require only sub-milliwatts of average power to function are being developed [4, 8, 24, 31]. Unfortunately, further evolution of such technologies is currently being moderated by the lack of continuous scalable energy sources that can be used to power and maintain them. Batteries, which remain the most adequate power choice, have not kept pace with the devices' demands, especially in terms of energy density [45]. In addition, their finite life span which necessitates regular replacement can be a very costly and cumbersome process. Consider, for instance, the difficulty of replacing batteries for a spatially-dense remotely-located wireless sensor network, or the risks involved in changing batteries for patients with implantable pace makers.

In light of such challenges and the low-power consumption of many new critical technologies, this last decade has witnessed a new evolution in energy harvesting technologies whereby the concept of micro-power generators (MPGs) was introduced [49, 55, 56]. MPGs

are compact energy harvesting devices that can transform the smallest amounts of available wasted ambient energy into electricity. When embedded with electronic devices, these generators can provide a continuous power supply permitting an autonomous operation process. Within the vast field of micro-power generation, vibratory energy harvesters (VEHs) have flourished as a major thrust area. Various devices have been developed to transform mechanical motions directly into electricity by exploiting the ability of active materials and some electromechanical mechanisms to generate an electric potential in response to mechanical stimuli and external vibrations [49, 55, 56].

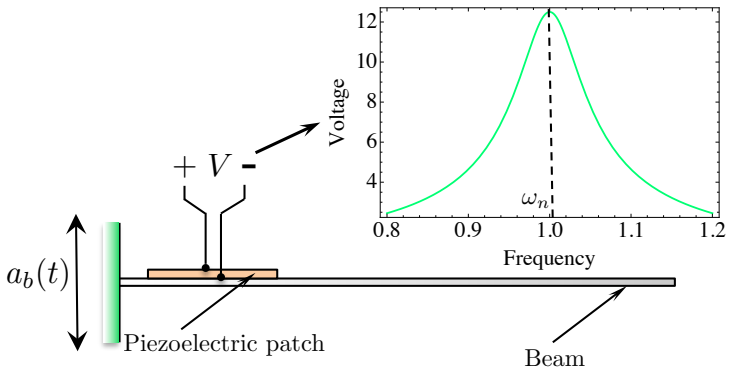

Figure 1.1: A schematic of a linear piezoelectric harvester and its voltage-frequency response.

The most prolific energy harvesting design consists of a cantilever beam subjected to base excitations as shown in Fig. 1.1. Attached to the beam near the clamped end are piezoelectric patches. External environmental excitations set the beam in motion producing large strains near the clamped end, which, in turn, produce a voltage difference across the piezoelectric patches. By designing the proper circuitry, this electric potential can be used to create a current that transfers energy from the environment to an electric device.

Key for efficient energy transduction is the ability to set the beam into large-amplitude oscillations. For an environmental excitation exhibiting harmonic fixed-frequency characteristics, large-amplitude beam deflections can be excited by tuning one modal frequency of the beam, usually the first, to be equal to the excitation frequency (resonance

condition). This tuning approach however, can, in many instances, be very difficult to achieve in realistic vibratory environments for the following reasons:

1. Linear VEHs similar to the cantilever beam shown in Fig. 1.1 have a very narrow frequency bandwidth. Small drifts in the excitation frequency around the harvester's fundamental frequency can easily occur due to small variations in the nature of the excitation source and/or changes in the design parameters of the harvester around their nominal values. This drops the already small energy output of VEHs even further making the energy harvesting process inefficient.

2. Most environmental excitations are not harmonic but have broad-band or non-stationary (time-dependent) characteristics in which the energy is distributed over a wide spectrum of frequencies or the dominant frequency vary with time. For instance, environmental excitations to which a bridge is subjected are generally random resulting from wind loadings whose frequency and intensity vary depending on the atmospheric conditions; and moving vehicles whose number, speed, weight, etc. vary at different times during a given day. Common sources for oscillations in microsystems have white noise characteristics normally due to non-equilibrium thermal fluctuations as well as shot and low-frequency noise [10, 59].

1.1 Current Solutions

To remedy this problem, some initial solutions called for the design of vibratory energy harvesters with tunable characteristics. Tuning mechanisms use passive/active design means to alter the fundamental frequency of the harvester to match the dominant frequency of the excitation [5, 9, 47, 50, 53, 53, 54, 58]. Following a number of research investigations, it became evident that tunable VEHs can only be utilized to account for slow drifts in the excitation's frequency and are not efficient under random or fast-varying frequency inputs [50]. In addition, tuning mechanisms usually require external power or complex design means. Others proposed solutions that utilize stacks of harvesters with different fundamen-

tal frequencies such that, at least, one will have a matching fundamental frequency and will, thereby, resonate and harvest energy from the corresponding excitation's component [5, 47, 53]. This, however, reduces the power density and adversely affects the scalability of the harvester.

A significant body of the current research on vibratory energy harvesting is focused on the concept of purposeful inclusion of stiffness nonlinearities for broadband transduction. When compared to their linear resonant counterparts, nonlinear energy harvesters have a wider steady-state frequency bandwidth, leading to the idea that they can be utilized to improve performance especially in random and non-stationary vibratory environments. The basic idea lies in altering the potential energy function of the harvesting system by introducing a nonlinear restoring force. In general, the nonlinearity can be introduced using external design means such as magnetic or mechanical forces [1, 2, 7, 12, 17, 18, 20, 35, 38, 40, 46, 57]. There are two different classes of these harvesters. The first is designed to exhibit a nonlinear resonant behavior similar to that of a mono-stable duffing oscillator with a hardening/softening nonlinearity [7, 35, 38]. As shown in Fig. 1.2, the nonlinearity bends the frequency-response curves to the left or to the right depending on its nature thereby extending the bandwidth of the harvester to a wider range of frequencies. However, the enhanced bandwidth is accompanied with the presence of regions of multiple stable solutions with different basins of attraction. As such, a mono-stable harvester is not always guaranteed to operate on the large-amplitude branch of solutions.

Examples of mono-stable VEHs include, but are not limited to, the magnetically-levitated inductive harvester proposed by Mann and Sims [35] and shown in Fig. 1.3 (a). This harvester comprises of two outer magnets to levitate a fluctuating central magnet. The nonlinearity is introduced in the form of the magnetic restoring force, which also enables the system to be tuned to a specific resonant frequency. Per Faraday's law, energy is generated as a result of the relative motion between the coil and the center magnet. Barton et al. [7] also proposed a mono-stable inductive VEH but in the form of a tip magnet attached to a cantilever beam, Fig. 1.3(b). When the beam oscillates, the magnet moves relative to a coil

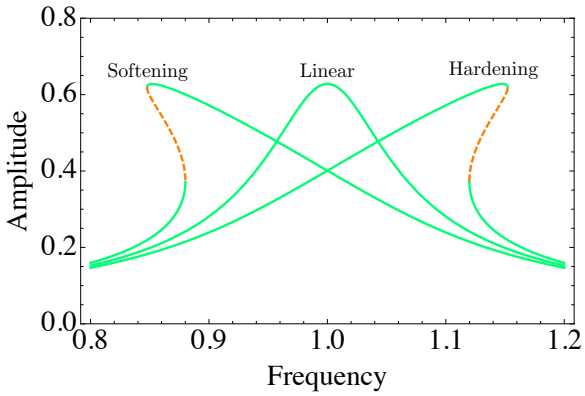

Figure 1.2: A typical steady-state frequency-response curve of a mono-stable energy harvester. Dashed lines represnt unstable solutions.

wound around an iron core generating a current in the coil.

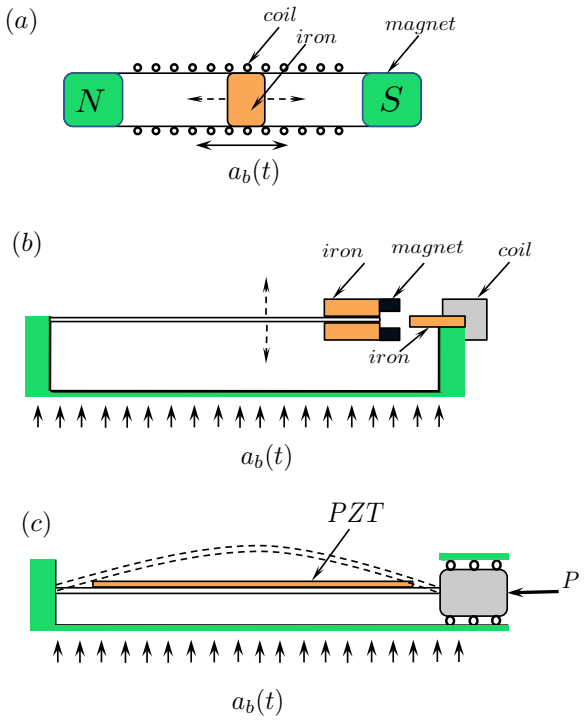

Figure 1.3: Schematics of different nonlinear energy havesters. (a,b) Inductive VEHs proposed in Refs. [35, 36] and Ref. [7], respectively; the linear stiffness and nonlinearity can be tuned by varying the distance between the magnets. (c) Piezoelectric VEH proposed in Ref. [38]; linear stiffness and nonlinearity can be tuned by varying an axial load, P. All devices can operate in the mono- and bi-stable configurations and $a_b(t)$ refers to the environmental base excitation.

Masana and Daqaq [38] also proposed a mono-stable axially-loaded piezoelectric clamped-clamped beam harvester as shown in Fig. 1.3 (c). The axial preload, which is kept below the critical buckling load, serves to tune the natural frequency of the beam and to introduce a cubic nonlinearity which depends on the magnitude of the axial load. The device harvests energy as a result of the excitation-induced deformation of a piezoelectric patch attached to the surface of the beam.

The second class of nonlinear harvesters is designed to have a double-well potential energy function exhibiting the response of a bi-stable oscillator as shown in Fig. 1.4 (b). The operation concept of this class, which has been initially proposed by Cottone et al. [12] and later studied by several researchers [7, 20, 38, 40, 57], is based on the widely-celebrated bi-stable magneto-elastic structure of Moon and Holmes [41]. While several variances of the device were proposed, the main concept of operation is very similar. As shown in Fig. 1.4(a), the device consists of a piezoelectric beam (harvester) with a ferroelectric tip oscillating between two magnets. For a certain separation range between those magnets, the system becomes bi-stable having a double-well potential energy function with two stable equilibria and one unstable saddle. When such a device is subjected to small input excitations, the dynamics remain confined to one potential well exhibiting a nonlinear resonant behavior similar to that of a regular mono-stable duffing oscillator. However, when enough energy is supplied to allow the dynamic trajectories to overcome the potential barrier and escape to the other potential well (inter-well motion) , the harvester can exhibit complex dynamic responses which can, under some conditions be favorable for energy harvesting [20, 57]. Masana and Daqaq [37] has investigated the relative response of a mono- and bi-stable VEHs based on the axially-loaded clamped-clamped piezoelectric beam design under harmonic excitations illustrating that the bi-stable harvester can only outperform the mono-stable design for some shapes of the potential energy function and for large base excitation levels.

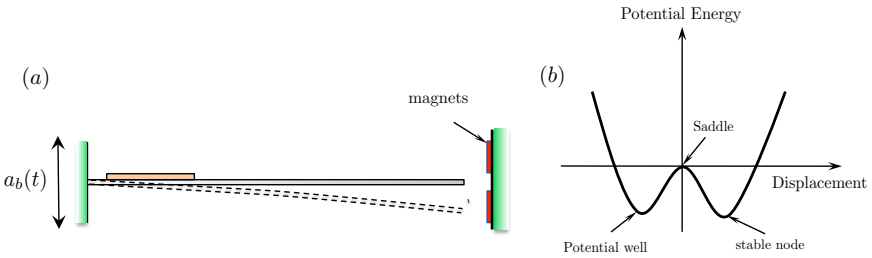

Figure 1.4: (a) Schematic of a bi-stable piezoelectric harvester. (b) Associated potential energy function.

1.2 Response to Random Excitations

While the purposeful introduction of nonlinearities has been aimed to resolve the issue of excitations' non-stationarities and randomness, the associated analyses and predicted power enhancements were, for the most part based, on the steady-state response which assumes a harmonic fixed-frequency excitation. As of today, we still do not have a clear understanding of how the nature of the excitation influences the output power, or what role stiffness nonlinearities play in the transduction of energy harvesters under random excitations. Still, it is not even well-understood whether the steady-state fixed-frequency analysis currently adopted in the literature is a valid performance indicator.

A few recent research studies have tried to address some of these unanswered questions by providing a clearer picture of how randomness and non-stationarities in the excitation influence the average power of nonlinear VEHs [3, 6, 14–16, 22, 23, 25, 43, 52]. Such studies were mainly focused on analyzing the response of a mono-stable Duffing harvester with a symmetric restoring force to white noise excitations. It was determined that the ratio between the period of the mechanical system and the time constant of the harvesting circuit plays an important role in characterizing the influence of the nonlinearity on the average power.

In one demonstration, Gammaitoni et al. [22] numerically and experimentally studied the response of a mono-stable piezoelectric energy harvester with symmetric potential to random excitations. They showed that, when the time constant of the harvesting circuit

is large, the root mean square (RMS) output voltage always decreases with the nonlinearity for a fixed linear stiffness. In another demonstration, Daqaq [14] considered an electromagnetic mono-stable VEH and formulated the Fokker-Plank-Kolmagorov (FPK) equation governing the evolution of the probability density function of the harvesters response under white noise. He showed that, when the inductance of the coil can be neglected (equivalent to having a very large time constant ratio), the PDF of the response can be separated into a function of the displacement and a function of the velocity, further proving that, under such conditions, the output power of the harvester is not even a function of the nonlinearity. Sebald et. al [51] confirmed these results experimentally by showing that the average output power levels of a linear and a nonlinear mono-stable Duffing-type harvesters are very close when both are excited with equivalent broadband noise.

In an extension to his earlier work, Daqaq [16] also showed that even when the time constant ratio is not large for both capacitive and inductive harvesters, the mean square voltage always decreases with the nonlinearity for a harvester with a symmetric restoring force. He concluded that, for two energy harvesters with equal linear stiffnesses, the one with zero nonlinear stiffness component always outperforms the one exhibiting a hardening nonlinear behavior. Recent research results by Green et al. [23] corroborated these findings but also showed that, although both the linear and nonlinear harvesters produce exactly similar power levels under white noise, the harvester with the nonlinear restoring force has a smaller RMS displacement when compared to the linear one making it better suited for applications with constrained space. In recent studies, Nguyen et al. and Halvorsen [26, 44] also demonstrated that the RMS voltage of the harvester is not a function of the nonlinearity when the time constant of the harvesting circuit is very small. Halvorsen [26] showed that, for intermediate values of the time constant, the RMS voltage of a mono-stable harvester with a hardening nonlinearity can never be larger than that of a linear harvester with equal linear stiffness.

The optimization of the electric load for mono-stable Duffing harvesters with a symmetric restoring force under white noise was discussed by Green et al. [23], who considered

an electromagnetic energy harvester with hardening nonlinearities and used statistical linearization to show that, when neglecting the inductance of the coil, the optimal load is not a function of the nonlinearity and is equal to that corresponding to the optimization of the linear problem.

The major portion of these studies investigate the response of mono-stable VEHs to excitations that can be approximated by a white noise process. However, due to the complexity of their response behavior under random inputs, bi-stable VEHs have received lesser attention. In one demonstration, Cottone et al. [12] analyzed the response of a bi-stable VEH to white and exponentially correlated noise excitations. They illustrated that, a bi-stable device can provide performance improvement over a linear device only when the time constant of the harvesting circuit is large. They explained that, since the nonlinear restoring force is only a function of the displacement, its maximum influence on the output power appears when the voltage is proportional to the displacement and not the velocity. This happens when the time constant of the harvesting circuit is large. By analytically solving the Fokker-Plank-Kolmogorov (FPK) equation which governs the probability density function (PDF) of the harvester's response, Daqaq [16] corroborated these findings and showed that, the mean power of a bi-stable harvester becomes independent of the nonlinearity when the time constant ratio, i.e., ratio between the period of the mechanical oscillator and the time constant of the harvesting circuit is large. Both researchers also showed that this condition is necessary but not sufficient to guarantee enhanced performance. They demonstrated that, for a given known noise intensity, the potential well of the harvester should be intricately designed to balance the rate of inter-well transitions (Kramer's rate) with wells' separation and the height of the potential barrier. Thus, it was concluded that, knowledge of the excitation's intensity is essential to design a bi-stable VEH which can outperform an equivalent linear one under white noise. This conclusion has also been confirmed by Litak et al. [34], Halvorsen [26], and Zho and Erturk [60]. Masana and Daqaq [39] illustrated experimentally that a properly designed bi-stable harvester outperforms the mono-stable one unless the variance of the input excitation is very small in which case both

configurations yield similar levels of output voltage.

1.3 Thesis Objectives and Organization

This thesis aims to delineate the influence of stiffness nonlinearities on the performance of energy harvesters operating in a white noise environment. Specifically, we first use statistical linearization techniques to investigate how the optimal power and associated electric load of mono-stable harvesters is influenced by the nonlinearity, the shape, and asymmetries in the restoring force. Results are then compared to an equivalent optimal linear harvesters and conclusions are drawn regarding utilizing the nonlinearity to enhance the performance of the harvester. Subsequently, we investigate the response of bi-stable VEHs to white noise excitations and focus on understanding whether their exists an optimal potential shape which maximizes the output power for a given noise intensity. Previously, Adhikari and Friswell [19] demonstrated using statistical linearization (SL) that the mean output power of a bi-stable symmetric VEH does not exhibit a maximum value at an optimal potential shape. They showed that the power always decreases as the depth and separation distance between the wells decreases. On the other hand, Cottone et. al [13] used a direct numerical integration of the stochastic differential equations to show that, under exponentially-correlated noise, the mean output power of a bistable symmetric harvester exhibits a maximum value at an optimal potential shape. They showed that this optimal shape corresponds to that maximizing the variance of the displacement. Here, we further investigate these finding using a combination of SL, numerical integration, and finite element solution of the FPK equation and arrive at some conclusions regarding the optimality of the shape of the potential function and the influence of the symmetry on the output power.

The rest of the thesis is organized as follows. Chapter 2 presents a general electromechanical model that can be used to study the response of nonlinear mono- and bi-stable energy harvesters. An exact solution of the FPK equation governing the response PDF is

then obtained for the linearized system and for the special case of a large time constant ratio. Statistical linearization techniques combined with an optimization algorithm are used to delineate the influence of the nonlinearity on the optimal electric load for both symmetric and asymmetric mono-stable potentials. Chapter 3 employs the method of statistical linearization in conjunction with finite element methods to solve the FPK equation for the approximate PDF of bi-stable harvesters. The approximate PDF is subsequently used to obtain the statistical averages of the response. The influence of potential shape and symmetry on the mean power of the harvester is analyzed. Finally, Chapter 4 presents the main conclusions.

Chapter 2

Response of Mono-stable Harvesters to White Noise

This chapter investigates the optimal response of linear and nonlinear monostable energy harvesters to white noise excitations. For a linear restoring force, the exact solution of the FPK equation is obtained and used to generate analytical expressions for the optimal mean power and associated electrical load. For a nonlinear restoring force, statistical linearization is utilized to obtain approximate analytical expressions for the statistical averages including the mean output power. An optimization algorithm is used to delineate the influence of the nonlinearity on the optimal electric load for both symmetric and asymmetric potentials.

2.1 Electromechanical Model

To achieve the objectives of this work, a basic model of a nonlinear VEH which consists of a mechanical oscillator coupled to an electric circuit through an electromechanical coupling mechanism is considered. The mechanism can either be piezoelectric, Fig. 2.1(a) or electromagnetic, Fig. 2.1(b). The piezoelectric energy harvester contains a critical part of piezoelectric layers, which is subjected to the vibrational beam. The deformation of the

beam would induce the strain in the piezoelectric materials, which further generate alternating voltage output across the electrodes. In the case of electromagnetic type harvester, it utilizes the movement of the magnets inside the coil to generate electrical power output.

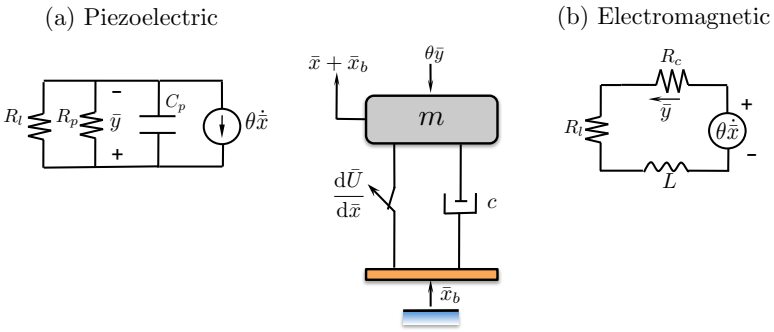

Figure 2.1: A simplified representation of a vibratory energy harvester.

To establish the mathematical model of the system, the equation of motion can be written as

$$m\ddot{\bar{x}} + c\dot{\bar{x}} + \frac{\mathrm{d}\bar{U}(\bar{x})}{\mathrm{d}\bar{x}} + \theta\bar{y} = -m\ddot{\bar{x}}_b, \tag{2.1a}$$

$$C_p\dot{\bar{y}} + \frac{\bar{y}}{R} = \theta\dot{\bar{x}}, (\text{piezoelectric}), \qquad L\dot{\bar{y}} + R\bar{y} = \theta\dot{\bar{x}}, (\text{electromagnetic}) \tag{2.1b}$$

where the dot represents a derivative with respect to time, τ. The variable $\bar{x}$ represents the relative displacement of the mass, m; c is a linear viscous damping coefficient; θ is a linear electromechanical coupling coefficient; $\ddot{\bar{x}}_b$ is the base acceleration; C_p is the capacitance of the piezoelectric element; L is the inductance of the harvesting coil, and $\bar{y}$ is the electric quantity representing the induced voltage in capacitive harvesters and the induced current in inductive ones. These are measured across an equivalent resistive load, R. In piezoelectric energy harvesters, the load, R, is the parallel equivalent of the piezoelectric resistance, R_p, and the load resistance, R_l, i.e., $R = \frac{R_l R_p}{R_l + R_p}$. In inductive harvesters, it represents the series equivalent of the load and coil resistance, R_c, i.e., $R = R_l + R_c$. The function $\bar{U}(\bar{x})$ represents the potential energy of the mechanical oscillator and is given in

the following general form:

$$\bar{U}(\bar{x}) = \frac{1}{2}k_1\bar{x}^2 + \frac{1}{3}k_2\bar{x}^3 + \frac{1}{4}k_3\bar{x}^4, \tag{2.2}$$

where k_1, k_2 and k_3 are, respectively, the linear, quadratic, and cubic nonlinearity coefficients appearing in the restoring force. The equations of motion can be further non-dimensionalized by introducing the following dimensionless quantities:

$$x = \frac{\bar{x}}{l_c}, \qquad x_b = \frac{\bar{x}_b}{l_c}, \qquad t = \tau\omega_n, \qquad y = \frac{C_p}{\theta l_c}\bar{y}\,(\text{piezoelectric}),\ y = \frac{L}{\theta l_c}\bar{y}\,(\text{electromagnetic}) \tag{2.3}$$

where l_c is a length scale, and $\omega_n = \sqrt{k_1/m}$ is the natural frequency of the mechanical oscillator when k_1 is greater than 0. With these transformations, the non-dimensional equations of motion can be expressed as

$$\ddot{x} + 2\zeta\dot{x} + \frac{\mathrm{d}U}{\mathrm{d}x} + \kappa^2 y = -\ddot{x}_b, \tag{2.4a}$$

$$\dot{y} + \alpha y = \dot{x}, \tag{2.4b}$$

and

$$\zeta = \frac{c}{2\sqrt{k_1 m}}, \qquad \kappa^2 = \frac{\theta^2}{k_1 C_p}\ (\text{capacitive}),\ \kappa^2 = \frac{\theta^2}{k_1 L}\ (\text{inductive}),$$
$$\lambda = \frac{k_2 l_c}{k_1}, \qquad \delta = \frac{k_3 l_c^2}{k_1}, \qquad \alpha = \frac{1}{RC_p\omega_n}(\text{piezoelectric}),\ \alpha = \frac{R}{L\omega_n}\ (\text{electromagnetic}).$$

where

$$\frac{\mathrm{d}U}{\mathrm{d}x} = x + \lambda x^2 + \delta x^3, \tag{2.5}$$

Here, ζ represents the mechanical damping ratio, κ is a linear dimensionless coupling coefficient, λ is the quadratic nonlinearity coefficient, δ is the cubic nonlinearity coefficient,

and α is the ratio between the period of the mechanical system and the time constant of the harvesting circuit. It is worth noting that, regardless of the electromechanical coupling mechanism, Equation (2.4), can be used to study the dynamics of any nonlinear mono- or bi-stable harvester with cubic nonlinearity. It is also worth mentioning that, in the non-dimensional form, the potential energy function and the restoring force depend only on λ and δ. This permits classifying energy harvesters, regardless of their coupling mechanism, into three major categories based on the shape of their potential energy function and the associated restoring force.

1. Linear when $\lambda = \delta = 0$: In such a case, the restoring force is a linear function of the displacement. Most linear VEHs are only linear within a certain range of operation. Large deformations and electromechanical coupling mechanisms can introduce small nonlinearities that are usually neglected to avoid complexities in the analysis.

2. Nonlinear mono-stable when $\delta > 0$ and $0 \leq \lambda < 2\sqrt{\delta}$: When $\delta > 0$ and $\lambda = 0$, the potential function is symmetric and has one minimum (mono-stable). The restoring force increases with the displacement and is said to be of the hardening type. When $\delta > 0$ and $0 < \lambda < 2\sqrt{\delta}$, the potential function remains mono-stable but loses its symmetry around the equilibrium as shown in Fig. 2.2(a).

3. Nonlinear bi-stable when $\delta > 0$ and $\lambda \geq 2\sqrt{\delta}$: Here, the potential function of the harvester has two potential wells separated by a potential barrier as depicted in Fig. 2.3.

In the case of bi-stable symmetric VEHs, the restoring force can also be written in the more convenient form

$$\frac{\mathrm{d}U}{\mathrm{d}x} = -x + \delta x^3, \tag{2.6}$$

in which case the potential function only depends on δ. As depicted in Fig. 2.4 when δ increases, the separation distance between the potential wells, $2\sqrt{1/\delta}$ and the height of the potential barrier at the saddle point, $1/(4\delta)$ both decrease. As such, the harvester approaches the mono-stable symmetric design when δ approaches a large number.

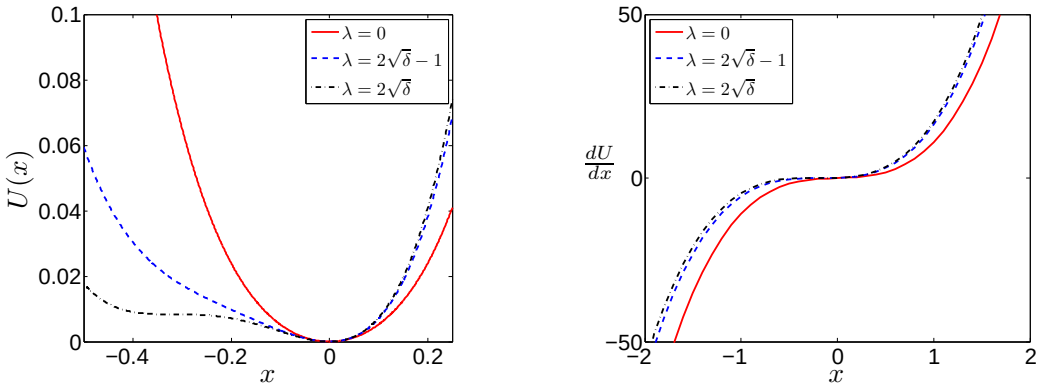

Figure 2.2: (a) Potential energy and (b) restoring force in nonlinear mono-stable VEHs

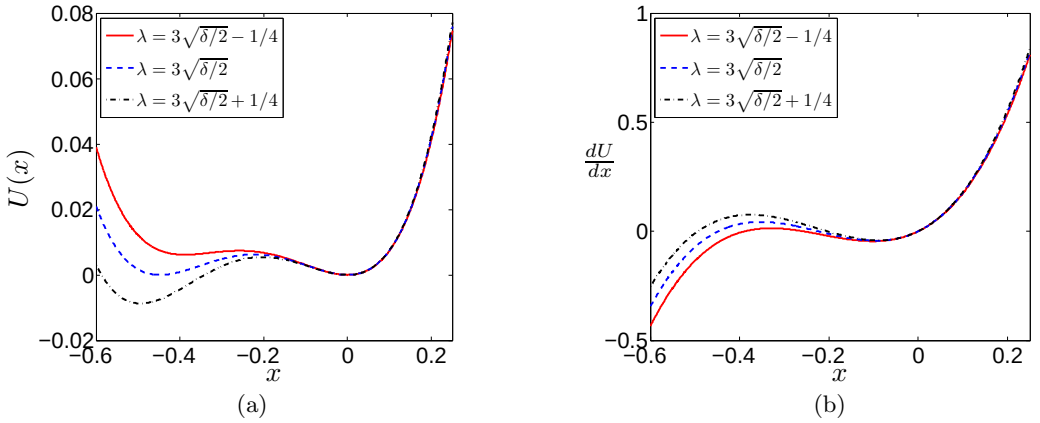

Figure 2.3: (a) Potential energy and (b) restoring force in nonlinear bi-stable VEHs.

2.2 Fokker-Plank-Kolmogorov (FPK) Equation

In the field of signal processing, white noise represents a random signal which exhibits a flat spectral density line in frequency domain. It has a wide application in science and technology, such as the disciplines of electrical engineering, acoustics, civil engineering and so on. In time domain, white noise displays random pattern which is unpredictable. However, By looking at such a signal in frequency domain, white noise is such a broad band process that covers an infinite band of frequencies, which represents a pure theoretical

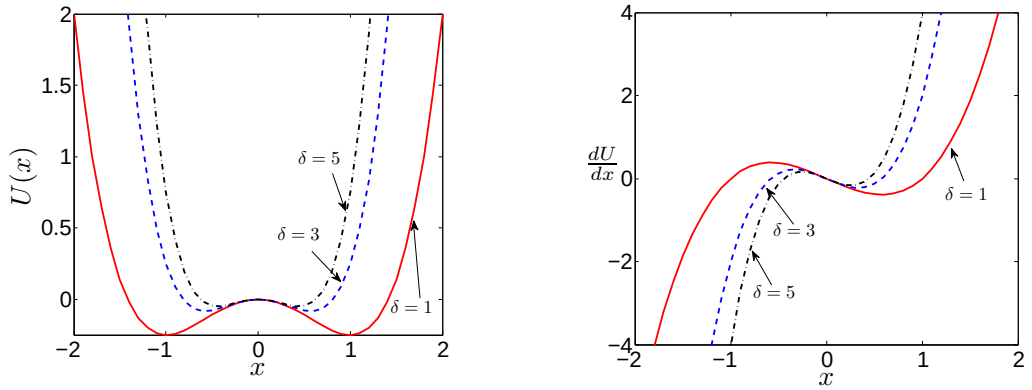

(a) (b)

Figure 2.4: Variation of (a) the potential energy $U(x)$ and (b) the restoring force $\frac{dU(x)}{dx}$ with the displacement for different values of the nonlinearity coefficient, δ

concept. In practical, a signal can be treated as white noise if its bandwidth is sufficiently larger than the frequencies of interest.

The excitation, $\ddot{x}_b$, to which the harvester is subjected is assumed to be a physical zero-mean Gaussian process with a small enough correlation time which tends to be zero. Gaussian noise is statistical noise that have the bell-shaped probability density function equal to normal distribution. Under this circumstances, $\ddot{x}_b$ can be approximated by a Gaussian white noise process such that[1]

$$\langle \ddot{x}_b(t) \rangle = 0, \qquad \langle \ddot{x}_b(t)\ddot{x}_b(s) \rangle = 2\pi S_0 \delta_0(s-t), \tag{2.7}$$

where $\langle\rangle$ denotes the expected value, S_0 is the spectral density of the process, and δ_0 is the dirac-delta function. The response statistics for the stochastic dynamics of Equation (2.4) can be generated by expressing the equations in the Itô stochastic form as [28, 29]

$$\mathrm{d}\mathbf{x}(t) = \mathbf{f}(\mathbf{x}, t)\mathrm{d}t + \mathbf{G}(\mathbf{x}, t)\mathrm{d}\mathbf{B}, \tag{2.8}$$

[1]The assumption of white noise is not as restrictive as it may appear. If the bandwidth of the excitation is sufficiently larger than that of the harvester's, then a random excitation can be safely considered to be white.

where $\mathbf{x} = (x_1, x_2, x_3)^T \equiv (x, \dot{x}, y)^T$, B is a Brownian motion process such that $\ddot{x}_b(t) = \mathrm{d}\mathbf{B}/\mathrm{d}t$ and

$$\mathbf{f}(\mathbf{x},t) = \begin{Bmatrix} x_2 \\ -2\zeta x_2 - \frac{dU}{dx_1} - \kappa^2 x_3 \\ -\alpha x_3 - x_2 \end{Bmatrix}, \qquad \mathbf{G}(\mathbf{x},t) = \begin{Bmatrix} 0 \\ -1 \\ 0 \end{Bmatrix}. \tag{2.9}$$

The solution of Equation (2.8) is determined by the evolution of the transition PDF, $P(\mathbf{x},t)$, which, in turn, is governed by the following FPK equation:

$$\begin{aligned} \frac{\partial P(\mathbf{x},t)}{\partial t} &= -\sum_{i=1}^{3} \frac{\partial}{\partial x_i}[P(\mathbf{x},t)\mathbf{f}_i(\mathbf{x},t)] \\ &\quad + \frac{1}{2}\sum_{i=1}^{3}\sum_{j=1}^{3} \frac{\partial^2}{\partial x_i \partial x_j}[P(\mathbf{x},t)(\mathbf{Q}\mathbf{G}\mathbf{G}^T)_{ij}], \\ P(\infty,t) &= P(-\infty,t) = 0, \end{aligned} \tag{2.10}$$

where

$$\mathbf{Q} = \begin{bmatrix} 0 & 0 & 0 \\ 0 & 2\pi S_0 & 0 \\ 0 & 0 & 0 \end{bmatrix}.$$

With the knowledge of $\mathbf{f}(\mathbf{x},t)$ and $\mathbf{G}(\mathbf{x},t)$, the FPK equation reduces to

$$\begin{aligned} \frac{\partial P(\mathbf{x},t)}{\partial t} &= -x_2\frac{\partial P(\mathbf{x},t)}{\partial x_1} + 2\zeta\frac{\partial (x_2 P(\mathbf{x},t))}{\partial x_2} + \left(\frac{dU}{dx_1} + \kappa^2 x_3\right)\frac{\partial P(\mathbf{x},t)}{\partial x_2} \\ &\quad + \alpha\frac{\partial (x_3 P(\mathbf{x},t))}{\partial x_3} + x_2\frac{\partial P(\mathbf{x},t)}{\partial x_3} + \pi S_0 \frac{\partial^2 P(\mathbf{x},t)}{\partial x_2^2}, \\ P(\infty,t) &= P(-\infty,t) = 0. \end{aligned} \tag{2.11}$$

Since, in our case, we are interested in the stationary response, the term $\frac{\partial P(\mathbf{x},t)}{\partial t}$ is

set to zero; thus, Equation (2.11) can be rewritten as

$$-x_2\frac{\partial P(\mathbf{x})}{\partial x_1}+2\zeta\frac{\partial(x_2P(\mathbf{x}))}{\partial x_2}+\left(\frac{dU}{dx_1}+\kappa^2x_3\right)\frac{\partial P(\mathbf{x})}{\partial x_2}+\alpha\frac{\partial(x_3P(\mathbf{x}))}{\partial x_3}+x_2\frac{\partial P(\mathbf{x})}{\partial x_3}+\pi S_0\frac{\partial^2P(\mathbf{x})}{\partial^2x_2}=0. \tag{2.12}$$

Upon solving Equation (2.12) for $P(\mathbf{x})$, the response statistics can then be obtained via

$$\left\langle\prod_{i=1}^{3}x_i^{k_i}\right\rangle=\int_{-\infty}^{\infty}\int_{-\infty}^{\infty}\int_{-\infty}^{\infty}\prod_{i=1}^{3}x_i^{k_i}P(\mathbf{x})\mathrm{d}x_1\mathrm{d}x_2\mathrm{d}x_3, \tag{2.13}$$

where $k_i=0,1,2,\ldots$.

2.3 Optimality of The Linear System

For the purpose of performance comparison, we first investigate the response statistics and the optimality of the design parameters for the linear harvester with $\lambda=\delta=0$. Since for linear systems, the response to a Gaussian input is also Gaussian, it is possible to obtain an exact stationary solution of Equation (2.11) in the general Gaussian form

$$P(x_1,x_2,x_3)=A\exp\left(\sum_{i,j=1}^{3}a_{ij}x_ix_j\right), \tag{2.14}$$

where A is a constant obtained via the following normalization scheme:

$$\int_{-\infty}^{\infty}\int_{-\infty}^{\infty}\int_{-\infty}^{\infty}P(x_1,x_2,x_3)\mathrm{d}x_1\mathrm{d}x_2\mathrm{d}x_3=1, \tag{2.15}$$

and the a_{ij} are attained by substituting Equation (2.14) into Equation (2.11), then forcing the solvability conditions. This yields

$$a_{ij}=-\frac{1}{2}\frac{|R|_{ij}}{|R|}, \tag{2.16}$$

where

$$R = \frac{2\pi S_0}{2\zeta(1+\alpha^2+2\alpha\zeta)+\kappa^2(\alpha+2\zeta)} \begin{bmatrix} 1+\alpha^2+2\alpha\zeta & 0 & \frac{1}{2} \\ 0 & \frac{1+\alpha^2+2\alpha\zeta+\kappa^2}{2} & \frac{\alpha}{2} \\ \frac{1}{2} & \frac{\alpha}{2} & \frac{1}{2} \end{bmatrix}.$$

Here, $|R|$ and $|R|_{ij}$ are, respectively, the determinant and co-factors of R.

With the knowledge of the exact stationary probability function, the required response statistics can now be obtained using Equation (2.13). Of special importance are the mean square values of the displacement, velocity, and electric quantity which can be expressed as

$$\left\langle x_1^2 \right\rangle = \pi S_0 \frac{1+\alpha^2+2\alpha\zeta}{2\zeta(1+\alpha^2+2\alpha\zeta)+\kappa^2(\alpha+2\zeta)}, \tag{2.17a}$$

$$\left\langle x_2^2 \right\rangle = \pi S_0 \frac{1+\alpha^2+2\alpha\zeta+\kappa^2}{2\zeta(1+\alpha^2+2\alpha\zeta)+\kappa^2(\alpha+2\zeta)}, \tag{2.17b}$$

$$\left\langle x_3^2 \right\rangle = \pi S_0 \frac{1}{2\zeta(1+\alpha^2+2\alpha\zeta)+\kappa^2(\alpha+2\zeta)}. \tag{2.17c}$$

Using Equation (2.17c), the dimensional average power can also be expressed in the simple form

$$\langle \mathrm{P} \rangle = k_1 l_c^2 \omega_n \alpha \kappa^2 \langle x_3^2 \rangle, \tag{2.18}$$

Equations (2.18) can be utilized to investigate the optimal time constant ratio, α, of the linear VEH. This can be achieved by differentiating Equation (2.18) with respect to α, then solving for α_{opt} to obtain

$$\alpha_{opt} = \sqrt{1+\kappa^2}. \tag{2.19}$$

The preceding expression reveals that the optimal time constant ratio of the linear harvester is only dependent on the electromechanical coupling, κ. Using the definition of the time constant ratio, we conclude that the optimal equivalent resistance occurs at

$R_{opt} = 1/(C_p\omega_n\sqrt{1+\kappa^2})$ for a piezoelectric VEH, and at $R_{opt} = L\omega_n\sqrt{1+\kappa^2}$ for an inductive one.

2.4 Optimality of the Nonlinear System

2.4.1 The Special Case of a Large Time Constant Ratio

In this section, the effect of the nonlinearity on the optimal electric load is investigated. Due to its simplicity, the case of a large time constant ratio, α, is first discussed. This serves to represent the behavior when either L or C_p are very small. In fact, it is a common practice in the literature to neglect the inductance of the coils in electromagnetic harvesters, and, sometimes the capacitance of the piezoelectric element for simplicity, [15, 23, 35]. From a mathematical point of view, the circuit dynamics, Equation (2.4b), represents a first-order low-pass filter with the velocity being its input, the electric quantity, y, representing its output, and α characterizing the inverse of its time constant. When α is large, the bandwidth of the filter is large, and the circuit dynamics can be approximated via $\alpha y = \dot{x}$. This allows the dynamics of the coupled system, Equation (2.4a), to be reduced to the following form:

$$\ddot{x} + \zeta_{eff}\dot{x} + \frac{\mathrm{d}U}{\mathrm{d}x} = -\ddot{x}_b \tag{2.20}$$

where $\zeta_{eff} = 2\zeta + \kappa^2/\alpha$. For the reduced system, the PDF of the response can be obtained by solving a reduced FPK equation of the form

$$\begin{aligned} \frac{\partial P(\mathbf{x},t)}{\partial t} &= -x_2\frac{\partial P(\mathbf{x},t)}{\partial x_1} + 2\zeta_{eff}\frac{\partial (x_2 P(\mathbf{x},t))}{\partial x_2} + \left(\frac{\mathrm{d}U}{\mathrm{d}x_1}\right)\frac{\partial P(\mathbf{x},t)}{\partial x_2} + \pi S_0\frac{\partial^2 P(\mathbf{x},t)}{\partial x_2^2}, \\ P(\infty,t) &= P(-\infty,t) = 0, \end{aligned} \tag{2.21}$$

where $(x_1, x_2)^T \equiv (x, \dot{x})^T$. In the stationary sense, the transition probability function is time invariant, i.e. $\partial P(\mathbf{x},t)/\partial t = 0$ or $P(\mathbf{x},t) = P(\mathbf{x})$, and Equation (2.21) admits the

following stationary solution:

$$P(x_1, x_2) = A_1 \exp\left\{\frac{-\zeta_{eff}}{\pi S_0} U(x_1)\right\} \times A_2 \exp\left\{\frac{-\zeta_{eff}}{\pi S_0}\frac{x_2^2}{2}\right\}, \tag{2.22}$$

where $A_1^{-1} = \int_{-\infty}^{\infty} \exp\left\{\frac{-\zeta_{eff}}{\pi S_0} U(x_1)\right\} \mathrm{d}x_1$ and $A_2^{-1} = \int_{-\infty}^{\infty} \exp\left\{\frac{-\zeta_{eff}}{\pi S_0}\frac{x_2^2}{2}\right\} \mathrm{d}x_2$. Note that, the resulting PDF can be factored into a function of the displacement, x_1, and a function of the velocity, x_2. This implies that the displacement and velocity can be treated as two independent random variables. In such a case, the expected mean square value of the velocity, $\langle x_2^2 \rangle$, is independent of the displacement, nonlinearity, and the potential function altogether; and is given by

$$\langle \dot{x}^2 \rangle \equiv \langle x_2^2 \rangle = A_2 \int_{-\infty}^{\infty} x_2^2 \exp\left\{\frac{-\zeta_{eff}}{\pi S_0}\frac{x_2^2}{2}\right\} \mathrm{d}x_2 = \frac{\pi S_0}{\zeta_{eff}}. \tag{2.23}$$

Using the relation $y = \dot{x}/\alpha$ in conjunction with Equation (2.23), the expected mean square value of the electric quantity can then be written as

$$\langle y^2 \rangle \equiv \langle x_3^2 \rangle = \frac{\pi S_0}{\alpha^2 \zeta_{eff}}. \tag{2.24}$$

Equation (2.24) reveals that the expected value of the electric quantity, voltage in the case of piezoelectric harvesters, and current in the case of electromagnetic ones, is independent of the shape of the potential function leading to the conclusion that for large values of the time constant ratio α, no matter how the potential function of the harvester is altered, it has no influence on the average output power. This conclusion holds for all harvesters with nonlinearities appearing in the restoring force.

Referring back to Equation (2.17c), it can be noted that when $\alpha >> \zeta$, i.e., when L or C_p approaches a very small number, the mean square value of the electric output reduces to

$$< x_3^2 >= \frac{\pi S_0}{\alpha^2 \zeta_{eff}}, \tag{2.25}$$

which is equivalent to Equation (2.24). This illustrates that the linear and nonlinear system have similar expressions for the electric quantity when α is large. Thus, the optimal load is the same for both cases as given by Equation (2.19). In dimensional terms, since C_p and L approach zero when α is large, R_{opt} approaches short circuit in electromagnetic VEHs, and approaches open circuit in piezoelectric ones.

It is worth noting that, while the variance of the electric quantity is independent of the nonlinearity as previously described, the variance of the displacement still decreases with the nonlinearity as discussed earlier in Ref. [23]. This implies that the nonlinearity helps produce the same average power but for a smaller variance in the displacement. Based on this result, the authors of Ref. [23] concluded that the nonlinearity can help produce a more compact device. However, this conclusion should be approached with caution since a reduction in variance does not necessarily prevent the instantaneous displacement from being large at some instants in time.

2.4.2 The General Case of Any Time Constant Ratio

When the time constant ratio is not necessarily large and the restoring force has a nonlinear dependence on the displacement, an exact solution of the FPK equation, Equation (2.11), is not easily attainable even in the stationary sense. The reason being that, even when the input excitation is Gaussian, the response PDF will deviate from the Gaussian distribution depending on the strength of the nonlinearity. To approximate the response statistics in such a scenario, it is common to seek approximate response statistics. One approach is based on statistically linearizing the governing equation of motion, Equation (2.4a). For the mono-stable nonlinear system at hand, methods of statistical linearization are capable of providing accurate response statistics for weakly nonlinear systems subjected to Gaussian excitations of moderate intensity. For a better understanding of the results, the case of a symmetric mono-stable potential is first considered.

2.4.2.1 Symmetric Potential

When the potential function is symmetric, the nonlinear equation of motion can be replaced by an equivalent linear system in the form

$$\begin{aligned} &\ddot{x} + 2\zeta\dot{x} + \omega_e^2 x + \kappa^2 y = -\ddot{x}_b, \\ &\dot{y} + \alpha y = \dot{x}, \end{aligned} \tag{2.26}$$

where $\omega_e^2 x$ is an equivalent linear restoring force that best approximates the nonlinear restoring force of Equation (2.4a). To obtain the unknown coefficient, ω_e^2, we minimize the main square error, E, between the actual restoring force and its linear equivalent, i.e., we let

$$\frac{\partial\langle E^2\rangle}{\partial\omega_e^2} = 0, \qquad \frac{\partial^2\langle E^2\rangle}{\partial(\omega_e^2)^2} > 0, \tag{2.27}$$

where $\langle E^2\rangle = \langle(\omega_e^2 x - x - \delta x^3)^2\rangle$. This yields

$$(\omega_e^2 - 1)\langle x^2\rangle - \delta\langle x^4\rangle = 0, \qquad \langle x^2\rangle > 0, \tag{2.28}$$

To find an approximate analytical expression for ω_e^2, the fourth order statistical moment of the displacement is approximated as $\langle x^4\rangle \approx 3\langle x^2\rangle^2$, which yields

$$\omega_e^2 = 1 + 3\delta\langle x^2\rangle. \tag{2.29}$$

With the knowledge of ω_e^2, the response statistics associated with the equivalent linear system, Equation (2.26), can now be obtained in a manner similar to that described in Section 2.3, resulting in the following expression:

$$\left\langle x^2\right\rangle = \left\langle x_1^2\right\rangle = \frac{\pi S_0}{1 + 3\delta\langle x_1^2\rangle} \frac{1 + 3\delta\langle x_1^2\rangle + \alpha^2 + 2\alpha\zeta}{2\zeta(1 + 3\delta\langle x_1^2\rangle + \alpha^2 + 2\alpha\zeta) + \kappa^2(\alpha + 2\zeta)}, \tag{2.30a}$$

$$\left\langle \dot{x}^2\right\rangle = \left\langle x_2^2\right\rangle = \pi S_0 \frac{1 + 3\delta\langle x_1^2\rangle + \alpha^2 + 2\alpha\zeta + \kappa^2}{2\zeta(1 + 3\delta\langle x_1^2\rangle + \alpha^2 + 2\alpha\zeta) + \kappa^2(\alpha + 2\zeta)}, \tag{2.30b}$$

$$\left\langle y^2 \right\rangle = \left\langle x_3^2 \right\rangle = \pi S_0 \frac{1}{2\zeta(1 + 3\delta\langle x_1^2\rangle + \alpha^2 + 2\alpha\zeta) + \kappa^2(\alpha + 2\zeta)}. \tag{2.30c}$$

and the dimensionless average power, $\langle \mathrm{P} \rangle = \alpha \langle x_3^2 \rangle$. Since the coefficient ω_e^2 still depends on the unknown variance of the displacement of the original nonlinear system, it is still necessary to approximate $\langle x_1^2 \rangle$. To achieve this goal, two approaches are commonly adopted in the literature. In the first approach, $\langle x_1^2 \rangle$ is approximated using the variance of the linear system, in other words, using Equation (2.17a). In the second approach, Equation (2.30a) is solved for $\langle x_1^2 \rangle$ and then substituted into Equation (2.30c). Naturally, the second approach is more accurate but involves the solution of a six order polynomial in $\langle x_1^2 \rangle$.

To investigate the accuracy of both approaches, variation of $\langle x_1^2 \rangle$ with the nonlinearity is compared to a numerical integration of the stochastic differential equations, Equations (2.8), as depicted in Fig. 2.5. It is evident that using the approximate variance based on the linear system, Equation (2.17a), to approximate $\langle x_1^2 \rangle$, yields results that significantly underestimates the numerical simulations especially for larger values of δ. Thus, the exact variance as obtained by solving Equation (2.30a) is used in this work to approximate the electric quantity and average output power.

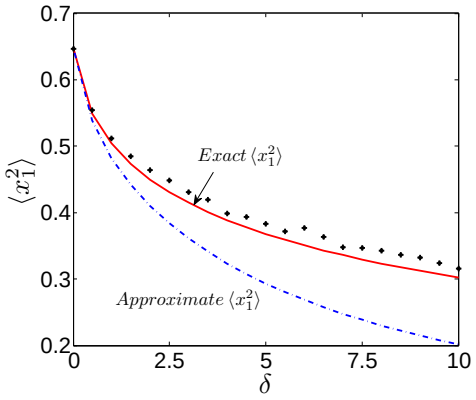

Figure 2.5: Variation of $\langle x^2 \rangle$ with the nonlinearity, δ, obtained for $\kappa = 0.65$, $\alpha = 0.5$, $\zeta = 0.01$, and $S_0 = 0.04$. Asterisks represent solutions obtained via numerical integration.

To investigate the optimal electric load embedded within the time constant ratio,

α, the equation $\frac{\partial \langle \mathrm{P} \rangle}{\partial \alpha_{opt}} = 0$ is solved for α_{opt} subject to the condition $\frac{\partial^2 \langle \mathrm{P} \rangle}{\partial \alpha_{opt}^2} < 0$. Results are shown in Fig. 2.6 illustrating that the optimal power always decreases with the nonlinearity regardless of the excitation spectral density. The optimal time constant ratio, on the other hand, increases with the magnitude of the nonlinearity.

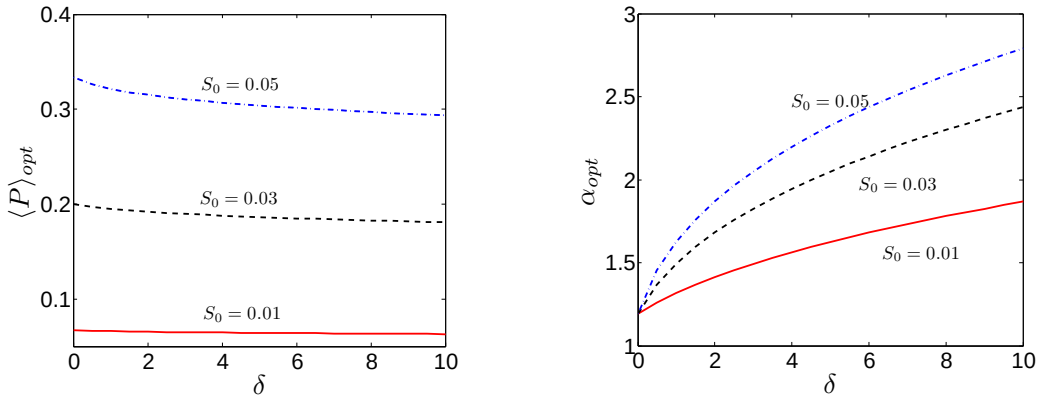

Figure 2.6: Variation of (a) optimal $\langle \mathrm{P} \rangle$ and (b) optimal α with the nonlinearity, δ for different values of S_0. Results are obtained for $\kappa = 0.65$ and $\zeta = 0.01$.

To put these non-dimensional quantities in a better perspective, we use the parameter values of the electromagnetic generator studied by Green et al. [23]. In their paper, the authors neglected the influence of the inductance on the power and found that the optimal load and power do not depend on the nonlinearity. This is the same conclusion we arrived at in Section 2.4.1. Upon dimensionalizing Equation (2.20), we arrive at the same power and optimal load expressions presented in Ref. [23]. These are given by

$$\langle \mathrm{P} \rangle_{opt} = \frac{\pi S_0 \theta^2 R_L}{2\zeta\omega_n (R_L + R_c)^2 + \frac{\theta^2 (R_L + R_c)}{m}}, \tag{2.31}$$

$$R_{l_{opt}} = \frac{\sqrt{(2\zeta\omega_n R_c)^2 + 2\zeta\omega_n R_c \theta^2}}{2\zeta\omega_n m}. \tag{2.32}$$

Clearly, the above expressions are independent of the nonlinearity. However, as shown in Fig. 2.7, if the inductance of the coil is not sufficiently small, the optimal power and

associated electric load are actually a function of the nonlinearity. When L is as small as 0.01 H, there is a clear dependence of the optimal power on both the inductance and the nonlinearity. Thus, by neglecting the inductance, the harvester operates away from its optimal conditions which reduces the average output power. It is worth noting that an inductance value as large as 0.08 H was reported in Ref. [36] for an actual electromagnetic energy harvester.

The preceding discussion clearly illustrates that the mono-stable Duffing harvester with a symmetric potential always produces lower average power than its linear counterpart with equivalent linear stiffness. Thus, even the unintentionally introduced hardening nonlinearities commonly seen in the first mode dynamics of beams, will inadvertently reduce the average output power of the harvester when operated in a white noise environment. Furthermore, it is shown that the optimal load has a clear dependence on the nonlinearity when L and C_p are not sufficiently small. As such, extreme caution should be practiced before neglecting the inductance of the coil or the capacitance of the piezoelectric element while performing optimization analysis as this may yield suboptimal results.

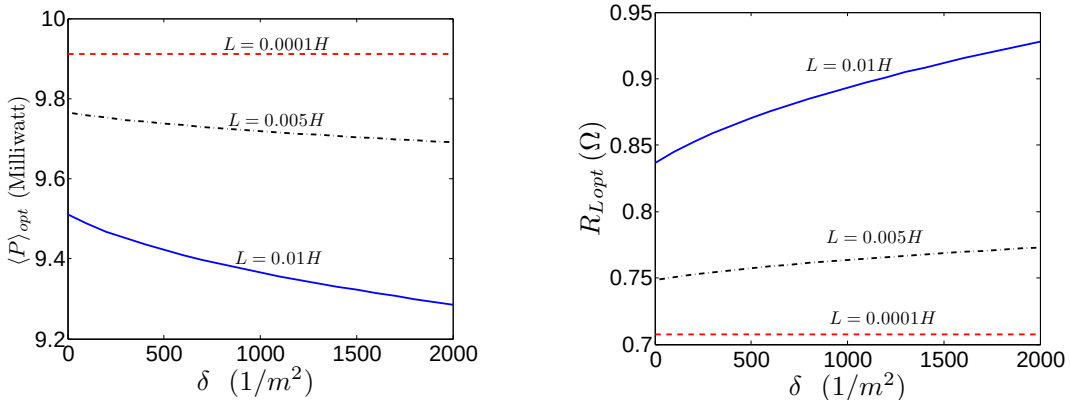

Figure 2.7: Variation of (a) optimal $\langle \mathrm{P} \rangle$ and (b) optimal R_L with the nonlinearity δ for $\omega_n = 40$ rad/s, $\theta = 0.2$ V$\cdot$ s/m, $m = 0.02$ kg, $\zeta = 0.05$, $S_0 = 1$ Watt/Hz and $R_c = 0.5\,\Omega$.

2.4.2.2 Asymmetric Potential

In many cases, the potential energy function of nonlinear mono-stable harvesters is asymmetric due to asymmetries in the nonlinear restoring force. For instance, structural imperfections, initial curvature, and added masses produce a quadratic nonlinearity in beam-type harvesters. Additionally, in the process of intentionally introducing nonlinearities to the harvester's through external design mechanisms, it is often difficult to create a perfectly symmetric restoring force.

Since the potential energy is no longer symmetric, harvesters with both quadratic and cubic nonlinearity do not necessarily have a zero mean value of displacement $\langle x \rangle \neq 0$ [48]. To account for this, we introduce the following transformation:

$$x(t) = x_0(t) + \langle x \rangle, \tag{2.33}$$

where $x_0(t)$ is the dynamics measured with respect to the mean of $x(t)$. Next, to statistically linearize the asymmetric system, we seek a linear restoring force that best approximates the nonlinear one in the form

$$\frac{\mathrm{d}U}{\mathrm{d}x} = \omega_{eq}^2 x_0 + b, \tag{2.34}$$

where b is introduced to account for a possible shift in the approximate linear force due to asymmetries in the original nonlinear restoring force. With that, the equivalent linear system can be written as

$$\ddot{x}_0 + 2\zeta\dot{x}_0 + \omega_{eq}^2 x_0 + b + \kappa^2 y = -\ddot{x}_b, \tag{2.35a}$$

$$\dot{y} + \alpha y = \dot{x}. \tag{2.35b}$$

To obtain the unknown coefficient, ω_{eq}^2, we minimize the main square error, E, between the

actual restoring force and its linear equivalent, i.e., we let

$$\frac{\partial\langle E^2\rangle}{\partial\omega_{eq}^2}=0, \qquad \frac{\partial\langle E^2\rangle}{\partial b}=0, \tag{2.36}$$

where $\langle E^2\rangle=\langle((x+\lambda x^2+\delta x^3)-(\omega_{eq}^2(x-\langle x\rangle)+b))^2\rangle$.

subject to

$$\frac{\partial^2\langle E^2\rangle}{\partial(\omega_{eq}^2)^2}>0, \qquad \frac{\partial^2\langle E^2\rangle}{\partial(\omega_{eq}^2)^2}\frac{\partial^2\langle E^2\rangle}{\partial b^2}-\left(\frac{\partial^2\langle E^2\rangle}{\partial\omega_{eq}^2\partial b}\right)^2>0. \tag{2.37}$$

By taking the statistical average of both sides of Equations (2.35a) and (2.35b), it can be shown that $b=\langle-\ddot{x}_b\rangle=0$, and $\langle y\rangle=0$. Furthermore, by assuming that the response PDF follows a Gaussian process, the higher-order moments can be approximated via

$$\langle x^3\rangle\approx 3\langle x\rangle\langle x^2\rangle-2\langle x\rangle^3, \tag{2.38}$$

$$\langle x^4\rangle\approx 3\langle x^2\rangle^2-2\langle x\rangle^4. \tag{2.39}$$

Substituting Equations (2.38) and (2.39) into Equation (2.36), and solving for ω_{eq}^2 and b yields

$$\omega_{eq}^2=3\delta\langle x^2\rangle+2\lambda\langle x\rangle+1, \tag{2.40}$$

$$b=3\delta\langle x\rangle\langle x^2\rangle-2\delta\langle x\rangle^3+\lambda\langle x^2\rangle+\langle x\rangle=0. \tag{2.41}$$

It is worth noting that, in the case of the asymmetric potential, ω_{eq}^2 depends on the nonzero mean value of x which can be obtained using Equation (2.41).

Repeating similar steps to those described in Section 2.4.2.1, the important response statistics can be expressed as

$$\langle x^2\rangle=\langle x_1^2\rangle=\frac{\pi S_0}{\omega_{eq}^2}\frac{\omega_{eq}^2+\alpha^2+2\alpha\zeta}{2\zeta(\omega_{eq}^2+\alpha^2+2\alpha\zeta)+\kappa^2(\alpha+2\zeta)}+\langle x_1\rangle^2, \tag{2.42a}$$

$$\langle \dot{x}^2 \rangle = \langle x_2^2 \rangle = \pi S_0 \frac{\omega_{eq}^2 + \alpha^2 + 2\alpha\zeta + \kappa^2}{2\zeta(\omega_{eq}^2 + \alpha^2 + 2\alpha\zeta) + \kappa^2(\alpha + 2\zeta)}, \tag{2.42b}$$

$$\langle y^2 \rangle = \langle x_3^2 \rangle = \pi S_0 \frac{1}{2\zeta(\omega_{eq}^2 + \alpha^2 + 2\alpha\zeta) + \kappa^2(\alpha + 2\zeta)}. \tag{2.42c}$$

and the dimensionless average power is given by, $\langle \mathrm{P} \rangle = \alpha \langle x_3^2 \rangle$.

Figure 2.8 depicts variation of average power with δ for different values of λ as obtained via statistical linearization and long-time integration of the original equations of motion. Good qualitative agreement between the statistical linearization results and the numerical integration is observed further validating the approximate results. It is also evident that the average power increases as λ is increased, i.e., as the restoring force becomes more asymmetric. The maximum value of the average power takes place at the extreme case of mono-stability where $\lambda = 2\sqrt{\delta}$. Beyond this value, the potential function becomes bi-stable. Most importantly, it can also be seen that, the average power of the mono-stable VEH with asymmetric potential can be larger than the linear VEH with $\delta = 0$ when λ is sufficiently large. This indicates that the asymmetry in the restoring force can help improve the average power of nonlinear mono-stable VEHs under white noise.

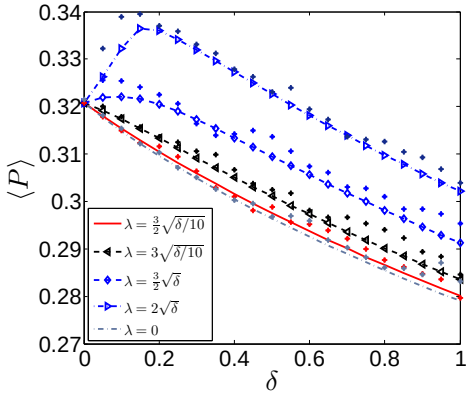

Figure 2.8: Variation of $\langle \mathrm{P} \rangle$ with the nonlinearity δ obtained for $\alpha = 0.5$, $\kappa = 0.65$, $\zeta = 0.01$ and $S_0 = 0.05$. Markers represent solutions obtained via numerical integration.

To better understand the influence of the time constant ratio on the output power

in the case of an asymmetric potential, we study variation of the mean square displacement and mean power with δ in the extreme case of $\lambda = 2\sqrt{\delta}$ for two different values of α as depicted in Figs. 2.9 and 2.10. It is clear that, for both values of α, the average power exhibits a maximum at some δ value. Furthermore, variation of the average power follows similar trends as the mean square displacement and is more pronounced for smaller values of α corresponding to large values of L or C_p. This trend can be explained by inspecting Equation (2.4b) and noting that, when α is small, the electric quantity (voltage of current) becomes directly proportional to the displacement.

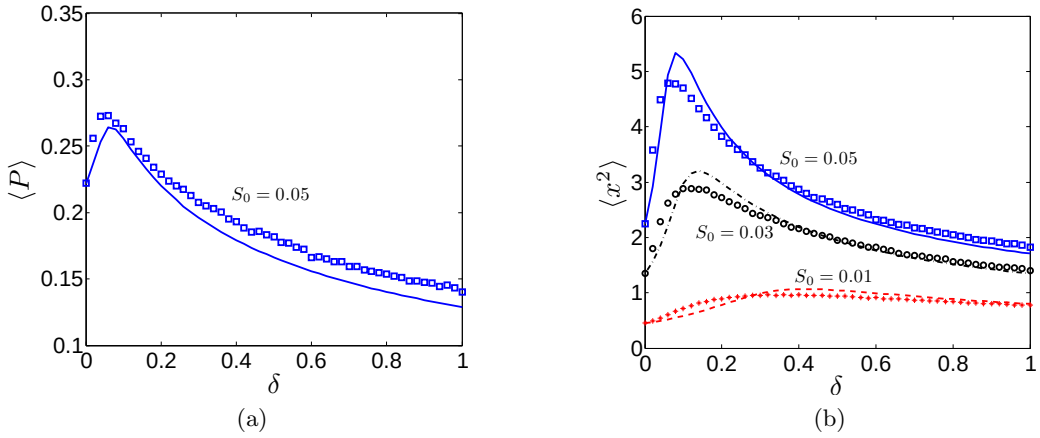

Figure 2.9: Variation of (a) $\langle \mathrm{P} \rangle$ and (b) $\langle x^2 \rangle$ with the non-linearity δ for $\lambda = 2\sqrt{\delta}$, $\alpha = 0.1$, $\kappa = 0.65$ and $\zeta = 0.01$. Markers represent solutions obtained via numerical integration.

Figures 2.9 and 2.10 also reveal that the average power is larger for $\alpha = 0.5$ than it is for $\alpha = 0.1$ indicating the presence of an optimal value. Figure 2.11 (a) investigates how this optimal value varies with δ for different values of the noise's spectral density. Results indicate that the optimal load decreases initially with δ, exhibits a minimum value then increases again as δ in increased further. The minimum value of α_{opt} corresponds to the maximum value of $\langle \mathrm{P} \rangle_{opt}$ as shown in Figs. 2.11 (b), (c) and (d). When compared to the symmetric potential ($\lambda = 0$) or the linear system ($\lambda = \delta = 0$), it is evident that the asymmetric potential produces higher optimal average power levels for all values of noise's spectral density.

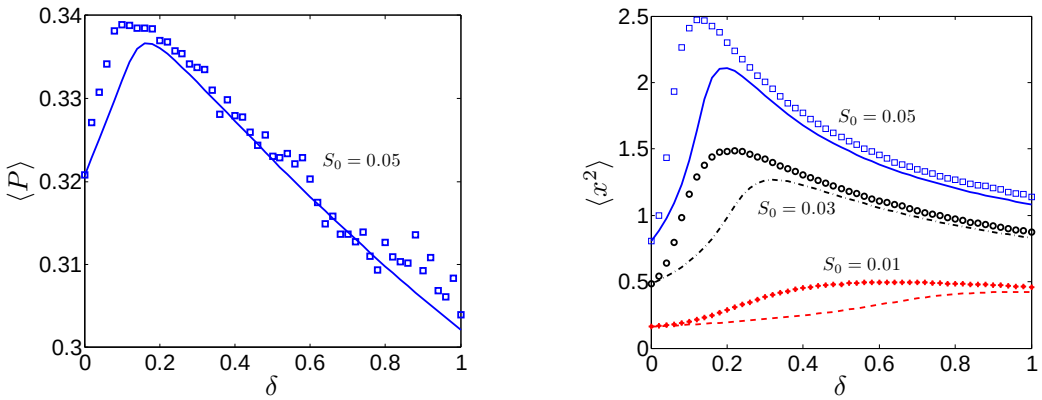

Figure 2.10: Variation of (a) $\langle \mathrm{P} \rangle$ and (b) $\langle x^2 \rangle$ with the nonlinearity δ for $\lambda = 2\sqrt{\delta}$, $\alpha = 0.5$, $\kappa = 0.65$ and $\zeta = 0.01$. Markers represent solutions obtained via numerical integration.

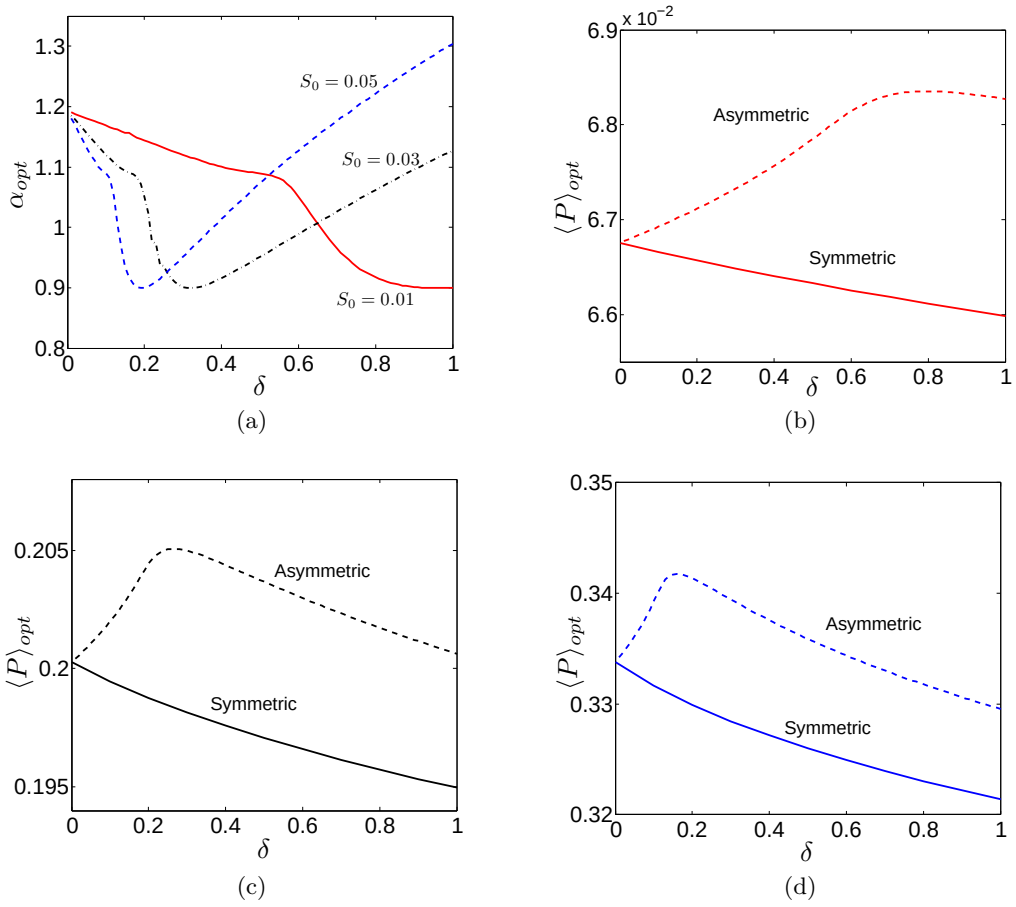

Figure 2.11: Variation of (a)α_{opt} and $\langle \mathrm{P} \rangle_{opt}$ with the nonlinearity δ for (b)$S_0 = 0.01$, (c)$S_0 = 0.03$ and (d)$S_0 = 0.05$. Results are obtained for $\kappa = 0.65$, $\zeta = 0.01$ and $\lambda = 2\sqrt{\delta}$.

Chapter 3

Response of Nonlinear Bi-stable Harvesters to White Noise

The exact solution of the FPK equation, which represents a linear partial differential equation with varying coefficients, is difficult to obtain in the case of a bi-stable potential, especially with the multi-dimensional nature of this problem. Hence, the solution must be approximated using other techniques. In this chapter, statistical linearization, direct numerical integration of the stochastic differential equations, and finite element solution of the FPK equation are utilized to approximate the probability density function (PDF) of the response. The PDF is then used to understand how the shape and symmetry of the potential energy function influence the mean output power of the harvester.

3.1 Statistical Linearization

Since Equation (2.12) is a linear partial differential equation (PDE) with varying coefficients, obtaining its exact solution, especially for this multi-dimensional problem, is not a simple task. As a result, some researchers attempted to approximate the response statistics of the bi-stable VEH using analytical methods [19]. Statistical linearization represents one common approach. To obtain the response statistics using the SL techniques for a bi-stable

VEH, it is assumed that the mean displacement of the response, $\langle x \rangle$, can be different from zero. Thus, the following transformation is introduced:

$$x(t) = x_0(t) + \langle x \rangle \tag{3.1}$$

to measure the dynamics, $x_0(t)$, with respect to the mean of $x(t)$. In SL, the nonlinear equation of motion is further replaced by an equivalent linear system in the form

$$\ddot{x}_0 + 2\zeta\dot{x}_0 + \omega_{eq}^2 x_0 + b + \kappa^2 y = -\ddot{x}_b, \tag{3.2a}$$

$$\dot{y} + \alpha y = \dot{x}, \tag{3.2b}$$

where $\omega_{eq}^2 x_0 + b$ is an equivalent linear restoring force that best approximates the nonlinear restoring force of Equation (2.4). To obtain the unknown coefficients, ω_{eq}^2 and b, we minimize the main square value of the error between the actual restoring force and its linear equivalent, i.e., we let

$$\frac{\partial \langle E^2 \rangle}{\partial \omega_{eq}^2} = 0, \qquad \frac{\partial \langle E^2 \rangle}{\partial b} = 0, \tag{3.3}$$

subject to

$$\frac{\partial^2 \langle E^2 \rangle}{\partial (\omega_{eq}^2)^2} > 0, \qquad \frac{\partial^2 \langle E^2 \rangle}{\partial (\omega_{eq}^2)^2} \frac{\partial^2 \langle E^2 \rangle}{\partial b^2} - \left(\frac{\partial^2 \langle E^2 \rangle}{\partial \omega_{eq}^2 \partial b} \right)^2 > 0.$$

where $\langle E^2 \rangle = \langle ((-x + \delta x^3) - (\omega_{eq}^2 (x - \langle x \rangle) + b))^2 \rangle$. This yields

$$\begin{gathered} (\omega_{eq}^2 + 1)(\langle x^2 \rangle - \langle x \rangle^2) - \delta(\langle x^4 \rangle - \langle x \rangle \langle x^3 \rangle) = 0, \\ b + 2\langle x \rangle - \delta \langle x^3 \rangle = 0. \end{gathered} \tag{3.4}$$

By taking the mean of both sides of Equations (3.2), we obtain

$$b = \langle -\ddot{x}_b \rangle = 0, \quad \langle y \rangle = 0. \tag{3.5}$$

Furthermore, using the property of the response statistics of a Gaussian process, the unknown higher-order moments are approximated as

$$\langle x^3\rangle = 3\langle x\rangle\langle x^2\rangle - 2\langle x\rangle^3, \qquad \langle x^4\rangle = 3\langle x^2\rangle^2 - 2\langle x\rangle^4. \tag{3.6}$$

Substituting Equation (3.6) into Equation (3.4), we obtain the following two equations:

$$\omega_{eq}^2 = -1 + 3\delta\langle x^2\rangle, \tag{3.7a}$$

$$\langle x\rangle(-1 + 3\delta\langle x^2\rangle - 2\delta\langle x\rangle^2) = 0. \tag{3.7b}$$

Equation (3.7a) indicates the effect of the nonlinearity can be approximated by an equivalent linear frequency which depends on the unknown variance of the displacement $\langle x^2\rangle$. Furthermore, Equation (3.7a) is subjected to the condition given by Equation (3.7b) which admits three possible solutions. One of these solutions is $\langle x\rangle = 0$, while the other two yield non-zero mean values. Physically, the first solution describes motions, which on average, has a zero mean about the unstable saddle. In other words, this solution refers to the harvester undergoing inter-well motions with zero mean around the unstable equilibrium point regardless of the shape of the potential function or the intensity of the excitation.

Next, the PDF of the linearized system of Equations (3.2a) and (3.2b) is obtained by solving the associated FPK equation. Since, for the equivalent linear system, the response to a Gaussian input is also Gaussian, it is possible to obtain an exact stationary solution of Equation (2.11) in the general Gaussian form

$$P(x_1, x_2, x_3) = A\exp\left(\sum_{i,j=1}^{3} a_{ij}x_i x_j\right), \tag{3.8}$$

where A is a constant obtained via the following normalization scheme:

$$\int_{-\infty}^{\infty}\int_{-\infty}^{\infty}\int_{-\infty}^{\infty} P(x_1, x_2, x_3)\mathrm{d}x_1\mathrm{d}x_2\mathrm{d}x_3 = 1, \tag{3.9}$$

and the a_{ij} are attained by substituting Equation (3.8) into Equation (2.11), then forcing the solvability conditions. This yields

$$a_{ij} = -\frac{1}{2}\frac{|R|_{ij}}{|R|}, \tag{3.10}$$

where

$$R = \frac{2\pi S_0}{2\zeta(\omega_{eq}^2 + \alpha^2 + 2\alpha\zeta) + \kappa^2(\alpha + 2\zeta)} \begin{bmatrix} \omega_{eq}^2 + \alpha^2 + 2\alpha\zeta & 0 & \frac{1}{2} \\ 0 & \frac{\omega_{eq}^2+\alpha^2+2\alpha\zeta+\kappa^2}{2} & \frac{\alpha}{2} \\ \frac{1}{2} & \frac{\alpha}{2} & \frac{1}{2} \end{bmatrix}.$$

Here, $|R|$ and $|R|_{ij}$ are, respectively, the determinant and co-factors of R.

With the knowledge of the exact stationary PDF, the required response statistics can now be obtained using Equation (2.13). Of special importance are the mean square values of the displacement, velocity, and electric quantity which are given by

$$\langle x^2\rangle = \frac{\pi S_0}{\omega_{eq}^2}\frac{\omega_{eq}^2 + \alpha^2 + 2\alpha\zeta}{2\zeta(\omega_{eq}^2 + \alpha^2 + 2\alpha\zeta) + \kappa^2(\alpha + 2\zeta)} + \langle x\rangle^2, \tag{3.11a}$$

$$\langle \dot{x}^2\rangle = \pi S_0\frac{\omega_{eq}^2 + \alpha^2 + 2\alpha\zeta + \kappa^2}{2\zeta(\omega_{eq}^2 + \alpha^2 + 2\alpha\zeta) + \kappa^2(\alpha + 2\zeta)}, \tag{3.11b}$$

$$\langle y^2\rangle = \pi S_0\frac{1}{2\zeta(\omega_{eq}^2 + \alpha^2 + 2\alpha\zeta) + \kappa^2(\alpha + 2\zeta)}. \tag{3.11c}$$

and the dimensionless average power, $\langle P\rangle = \alpha\langle y^2\rangle$. By solving Equations (3.7a), (3.7b), and (3.11a) together, the equivalent natural frequency, ω_{eq}^2, the mean displacement $\langle x\rangle$, and the mean square displacement $\langle x^2\rangle$ can be obtained. Subsequently, the mean square

velocity $\langle \dot{x}^2 \rangle$, and the mean square value of the electric quantity, $\langle y^2 \rangle$, which depend on ω_{eq}^2 can be calculated.

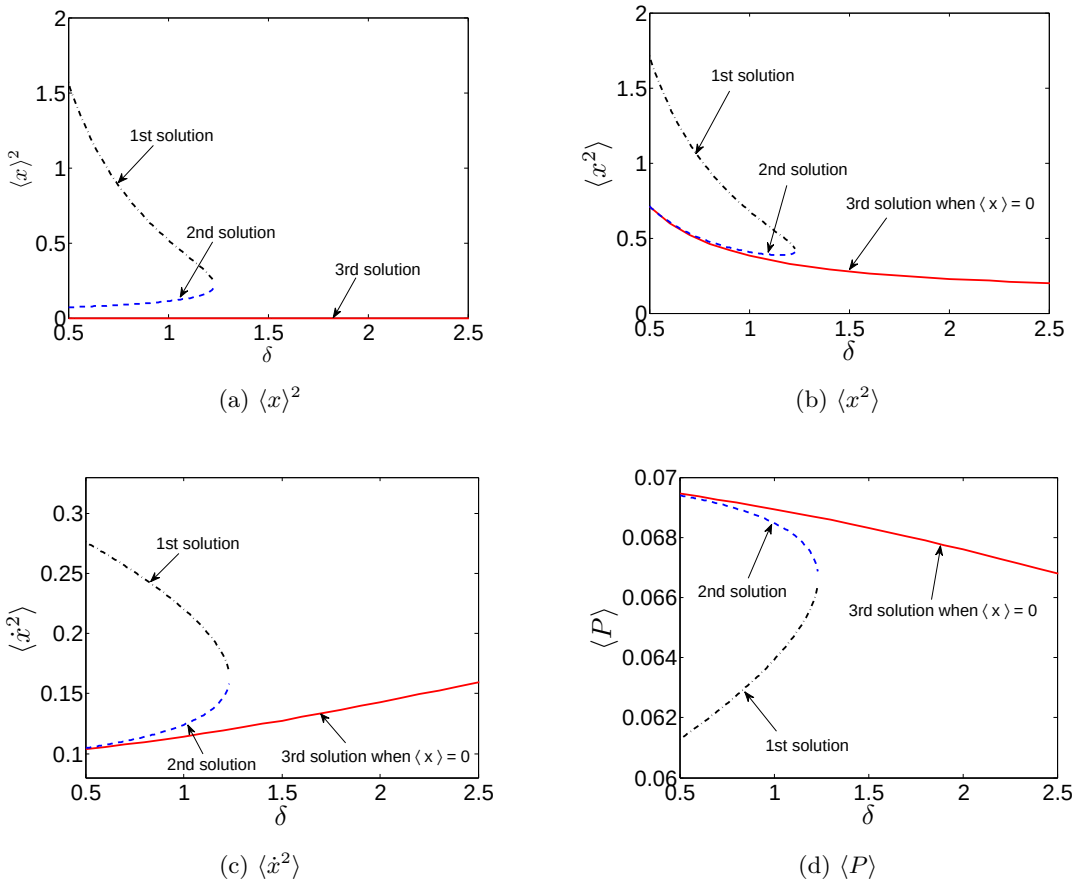

(a) $\langle x \rangle^2$ (b) $\langle x^2 \rangle$

(c) $\langle \dot{x}^2 \rangle$ (d) $\langle P \rangle$

Figure 3.1: Variation of $\langle x \rangle^2$, $\langle x^2 \rangle$, $\langle \dot{x}^2 \rangle$, and $\langle P \rangle$ with δ obtained for $\kappa = 0.65$, $\zeta = 0.01$, $\alpha = 0.5$, and $S_0 = 0.01$.

Using Equations (3.11a)- (3.11c), we study variation of $\langle x \rangle^2$, $\langle x^2 \rangle$, $\langle \dot{x}^2 \rangle$ and $\langle P \rangle$ with the nonlinearity coefficient δ as depicted in Fig. 3.1. Results illustrate that, in general, there are three possible branches of solution. The first two are associated with the non-zero mean displacement condition to reflect steady-state dynamic motions of the harvester that do not necessarily average to zero about the saddle point. These solutions only exist for small values of δ because the potential wells are too deep. When the intensity of the white noise is increased as depicted in Fig. 3.2, these solutions disappear at even smaller values

of δ. The third solution which exists over the entire domain of δ, and regardless of the noise intensity is associated with the zero mean displacement motion of the harvester. This solution yields the largest values of the mean power that always decrease as δ increases.

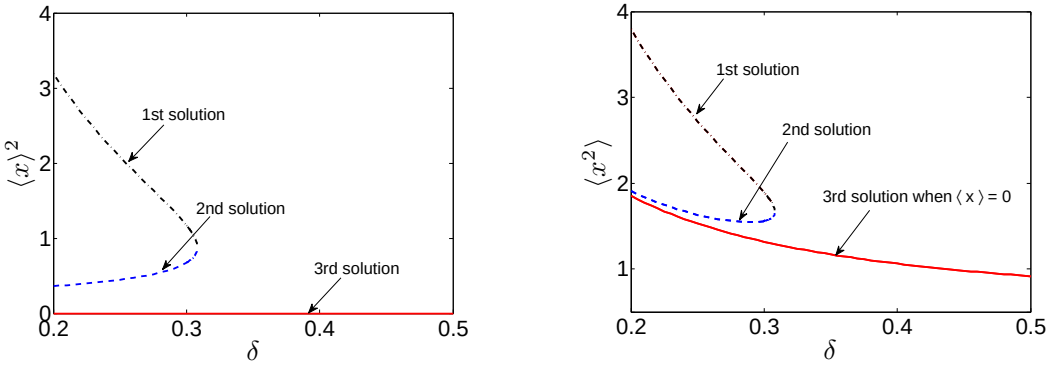

(a) $\langle x \rangle^2$ (b) $\langle x^2 \rangle$

Figure 3.2: Variation of $\langle x \rangle^2$ and $\langle x^2 \rangle$ with δ obtained for $\kappa = 0.65$, $\zeta = 0.01$, $\alpha = 0.5$, and $S_0 = 0.04$.

The presence of non-unique solutions at some values of δ as obtained using the SL approach is incorrect because the PDF of the response should be unique for any value of δ. As such, some, or all of the solutions obtained via the SL method are fictitious and do not reflect the actual long-time behavior of the system. In fact, the two branches of solution appearing for small values of δ are only a result of statistically linearizing the dynamics around the stable equilibria. These solutions state that, if the potential energy function is too deep, the dynamics can spend more time in one potential well versus the other yielding non-zero mean values of the displacement. However, we know that, under white noise, no matter what the shape of the potential function is, the dynamics will have zero mean value after a long enough time. Therefore, it is essential to validate these solutions against other, more accurate techniques, before studying the influence of the design parameters on the average output power of the system. To achieve this task, one possible solution is to integrate the stochastic differential equations numerically using some especially developed tools, e.g. the communication toolbox in Matlab. However, this approach is not very

accurate especially as we try to understand the dynamics for small values of δ, i.e., when the potential wells are very deep. In such a scenario, obtaining accurate response statistics via direct numerical integration of the stochastic equations of motion is very time consuming since the dynamic trajectories can take a very long time to escape a single potential well. This issue becomes especially prevalent when the variance of the excitation is small.

A more accurate approach is based on solving the FPK equation of the system analytically or numerically for the response PDF. Unfortunately, the exact solution of Equation (2.12), which represents a linear partial differential equation (PDE) with varying coefficients, is difficult to obtain for this multi-dimensional problem. Hence, the solution must be approximated using other techniques, among which FEM represents a good candidate. Finite element techniques become extremely beneficial as we try to understand the dynamics for small values of δ, i.e., when the potential wells are very deep.

3.2 Finite Element Analysis

In this section, we present a specially designed Finite Element technique to solve the FPK equation and compare the results to the SL approach [32]. Since the problem of solving Equation (2.12) using FEM is not a trivial one and cannot be readily solved using commercial softwares, we elect to provide some details to explain the process. Equation (2.12) contains 3 non-dimensional variables: the displacement x_1, the velocity x_2, and the electric output x_3. Since Equation (2.12) appears in its strong form, it is first converted to its weak form to facilitate the application of FEM. To achieve this goal, the Galerkin weighted residual method is adopted and Equation (2.12) is rewritten in the following form:

$$\mathscr{L}\left[P\left(\mathbf{x}\right)\right] = \mathcal{L}_1\left[P\left(\mathbf{x}\right)\right] + \mathcal{L}_2\left[P\left(\mathbf{x}\right)\right] = 0, \tag{3.12}$$

where $\mathscr{L}$ denotes a differential operator with $\mathscr{L}_1$ and $\mathscr{L}_2$ expressed as

$$\mathscr{L}_1 = -\sum_{i=1}^{3} \frac{\partial}{\partial x_i}[f_i(\mathbf{x})\cdot], \qquad \mathscr{L}_2 = \frac{1}{2}\sum_{i=1}^{3}\sum_{j=1}^{3}(\mathbf{Q}\mathbf{G}\mathbf{G}^T)_{ij}\frac{\partial^2}{\partial x_i \partial x_j}[\,], \tag{3.13}$$

For any arbitrary continuous weighting function $\phi(\mathbf{x})$ defined on a certain domain, R, Equation (3.12) can be rewritten as

$$\int_R \phi(\mathbf{x})\mathscr{L}_1[P(\mathbf{x})]d\tau + \int_R \phi(\mathbf{x})\mathscr{L}_2[P(\mathbf{x})]d\tau = 0, \tag{3.14}$$

where R defines the whole domain and $d\tau \equiv dx_1dx_2dx_3$. Using integration by parts, the first term in Equation (3.14) can be written as

$$\begin{aligned}\int_R \phi(\mathbf{x})\mathscr{L}_1[P(\mathbf{x})]d\tau &= -\sum_{i=1}^{3}\int_R \phi(\mathbf{x})\frac{\partial}{\partial x_i}[f_i(\mathbf{x})P(\mathbf{x})]d\tau \\ &= -\sum_{i=1}^{3}\int_{R'}[\phi(\mathbf{x})f_i(\mathbf{x})P(\mathbf{x})]_{x_{i1}}^{x_{i2}}d\tau' + \sum_{i=1}^{3}\int_R f_i(\mathbf{x})P(\mathbf{x})\frac{\partial}{\partial x_i}[\phi(\mathbf{x})]d\tau,\end{aligned} \tag{3.15}$$

Similarly, the second term of Equation (3.14) can be expressed as

$$\begin{aligned}&\int_R \phi(\mathbf{x})\mathscr{L}_2[P(\mathbf{x})]d\tau = \frac{1}{2}\sum_{i=1}^{3}\sum_{j=1}^{3}(\mathbf{QGG}^T)_{ij}\int_R \phi(\mathbf{x})\frac{\partial^2}{\partial x_i\partial x_j}[P(\mathbf{x})]d\tau \\ &= \frac{1}{2}\sum_{i=1}^{3}\sum_{j=1}^{3}(\mathbf{QGG}^T)_{ij}\left\{\int_{R'}[\phi(\mathbf{x})\frac{\partial}{\partial x_j}P(\mathbf{x})]_{x_{i1}}^{x_{i2}}d\tau' - \int_R \frac{\partial}{\partial x_i}[\phi(\mathbf{x})]\frac{\partial}{\partial x_j}[P(\mathbf{x})]d\tau\right\}.\end{aligned} \tag{3.16}$$

where R' and $d\tau'$ are the reduced domains excluding the variables upon which the integration is carried out, and x_{i2} and x_{i1} are the upper and lower bound of x_i respectively.

The region, R, which contains the variables x_1, x_2 and x_3, is of infinite span. In such a domain, the value of the probability density function $P(\mathbf{x})$ is very close to zero when any of the components of the vector $\mathbf{x}$ becomes large. This implies that $P(\mathbf{x})$ and its first derivative vanish at infinity leading to the elimination of the first terms of Equation (3.15) and Equation (3.16). With that, the weak form of Equation (3.14) is reduced to

$$\sum_{i=1}^{3}\int_R f_i(\mathbf{x})P(\mathbf{x})\frac{\partial}{\partial x_i}[\phi(\mathbf{x})]d\tau - \frac{1}{2}\sum_{i=1}^{3}\sum_{j=1}^{3}(\mathbf{QGG}^T)_{ij}\int_R \frac{\partial}{\partial x_i}[\phi(\mathbf{x})]\frac{\partial}{\partial x_j}[P(\mathbf{x})]d\tau = 0. \tag{3.17}$$

To find the unknown stationary PDF, $P(\mathbf{x})$, we apply the FEM to the formulated weak form of Equation (3.17). To achieve this goal, the corresponding region must satisfy the condition of integration over a finite domain which our problem lacks. To resolve this problem, we use the knowledge that the PDF, $P(\mathbf{x})$, approaches zero as the components of the vector $\mathbf{x}$ approach infinity. This allows us to truncate the infinite domain to a finite region out of which the PDF is assumed to be zero. In order to define the boundaries of this region, a direct numerical integration of the original stochastic differential equations is used to provide a rough estimate for the components of the vector $\mathbf{x}$ beyond which the PDF becomes very small.

Once the interior region is defined, it is discretized into a set of $n = 3$ dimensional element (cuboid element), which consists of $m = 2^n$ corner nodes. The integration over the finite domain of Equation (3.17) is further discretized as a sum of the integration over each element. The weighting function is selected to be the variation of the PDF, $\delta P(\mathbf{x})$. This yields

$$\begin{aligned}\sum_e \Bigg\{ \sum_{i=1}^{3} \int_e f_i(\mathbf{x}) P^e(\mathbf{x}) \frac{\partial}{\partial x_i}[\delta P^e(\mathbf{x})] d\tau \\ - \frac{1}{2} \sum_{i=1}^{3} \sum_{j=1}^{3} (\mathbf{Q}\mathbf{G}\mathbf{G}^T)_{ij} \int_e \frac{\partial}{\partial x_i}[\delta P^e(\mathbf{x})] \frac{\partial}{\partial x_j}[P^e(\mathbf{x})] d\tau \Bigg\} = 0,\end{aligned} \tag{3.18}$$

where $\sum_e$ denotes the sum of the integration over each element, $\int_e$ is the integration over each element, and P_e is the unknown PDF for the element e. The unknown PDF, $P_e(\mathbf{x})$, and the position dependent vector, $f_i(\mathbf{x})$, can be approximated as the sum of the nodal values multiplied by their corresponding shape functions; that is

$$P^e(\mathbf{x}) = \sum_{r=1}^{m} N_r(\mathbf{x}) P_r, \qquad f_i(\mathbf{x}) = \sum_{s=1}^{m} N_s(\mathbf{x}) f_i^s \qquad \frac{\partial}{\partial x_i}[P^e(\mathbf{x})] = \sum_{k=1} m \frac{\partial}{\partial x_i}[N_k(\mathbf{x}) \delta P_k], \tag{3.19}$$

where m represents the number of nodes of each element; P_r and P_k are the PDF evaluated at nodes r and k, respectively; $N_r(\mathbf{x})$, $N_s(\mathbf{x})$, and $N_k(\mathbf{x})$ are the shape functions evaluated

at nodes r,s, and k; respectively; and, finally, f_i^s is the value of f_i evaluated at node s.

The shape function, $N_r(\mathbf{x})$, $N_s(\mathbf{x})$, and $N_k(\mathbf{x})$ take a similar form and are chosen to be unity at nodes r, s and k [32]. For the sake of demonstration, we illustrate the shape function $N_r(\mathbf{x})$ which takes the form

$$N_r(\mathbf{x}) = \prod_{k=1}^{n} f_{kr}(x_k), \tag{3.20}$$

where $f_{kr}(x_k) = (x_{k_0} + dx_k - x_k)/dx_k$ when the x_k coordinate of node i lies in x_0, and $f_{kr}(x_k) = (x_k - x_{k_0})/dx_k$ when the x_k coordinate of node i lies in $x_0 + dx$, with x_{k_0} representing the k^{th} coordinate for the point x_0.

Next, Equation (3.19) is substituted into Equation (3.18), which yields

$$\begin{aligned}\sum_e \Bigg\{ \sum_{r=1}^{8}\sum_{k=1}^{8} \Bigg[\sum_{s=1}^{8}\sum_{i=1}^{3} \int_e f_i^s N_s N_r P_r \frac{\partial}{\partial x_i}[N_k \delta P_k] d\tau \\ - \frac{1}{2}\sum_{i=1}^{3}\sum_{j=1}^{3} (\mathbf{QGG}^T)_{ij} \int_e \frac{\partial}{\partial x_i}[N_k \delta P_k] \frac{\partial}{\partial x_j}[N_r P_r] d\tau \Bigg] \Bigg\} = 0,\end{aligned} \tag{3.21}$$

which upon further reduction can be written as

$$\sum_e \left\{ \sum_{r=1}^{8} k_{kr}^e P_r \right\} = \mathbf{0}, \tag{3.22}$$

where

$$k_{kr}^e = \sum_{s=1}^{8}\sum_{i=1}^{3} \int_e f_i^s N_s N_r \frac{\partial}{\partial x_i}[N_k] d\tau - \frac{1}{2}\sum_{i=1}^{3}\sum_{j=1}^{3} (\mathbf{QGG}^T)_{ij} \int_e \frac{\partial}{\partial x_i}[N_k] \frac{\partial}{\partial x_j}[N_r] d\tau. \tag{3.23}$$

Here, k^e represents the 8×8 element matrix, k_{kr}^e is the entry of stiffness matrix k^e in row k and column r, and P_r represents the rth entry of the column vector P^e. Although the integral in the element matrix k^e can be evaluated on the physical element in 3D coordinate system for the simple rectangular elements, isoparametric mapping is utilized in this paper

to perform the integration over the master element [11].

Because the stiffness matrix in Equation (3.23) is obtained through isoparametric mapping, the Gaussian quadrature method can be utilized to evaluate the terms inside the integration. It is worth mentioning that this is still a local matrix regarding only a single element, assembly of these local matrices is required by referring to the relation between local and global indices. Upon assembly of the global matrix, we obtain the following eigenvalue problem:

$$\mathbf{KP} = \mathbf{0}, \tag{3.24}$$

where $\mathbf{K}$ is a $n \times n$ singular matrix, $\mathbf{P}$ is a $n \times 1$ vector which represents the nodal PDFs at the global nodes, and n represents the number of global nodes. Equation (3.24) can be solved for the unknown vector $\mathbf{P}$ which can then be assembled to approximate the response PDF. Different from the equations usually encountered in solving Laplace's equation for structural problems, the right hand side of Equation (3.24) is equal to zero, for which the trivial solution $\mathbf{P} = \mathbf{0}$ is a candidate solution. However, this solution conflicts with the property of the PDF, which states that the integral of the PDF over the whole domain is unity; i.e., $\int_R P(\mathbf{x}) d\tau = 1$. Therefore, the non-trivial solutions are the only solutions considered. The resulting PDF can then be integrated numerically to obtain the response statistics using Equation (2.13).

3.3 Results of the Finite Element Analysis

Results of the FEM are shown in Fig. 3.3 which displays a cross-sectional view of the PDF for different sets of variables, $\{x_1, x_2\}$, $\{x_1, x_3\}$ and $\{x_2, x_3\}$, respectively. It is observed that the PDF has origin symmetry, which results from considering a symmetric potential function as depicted earlier in Fig. 2.4(a). The presence of two symmetric peaks near the potential wells implies that the dynamic trajectories have a higher but equal probability of being near the two potential wells of the bi-stable harvester for the given design parameters and noise intensity.

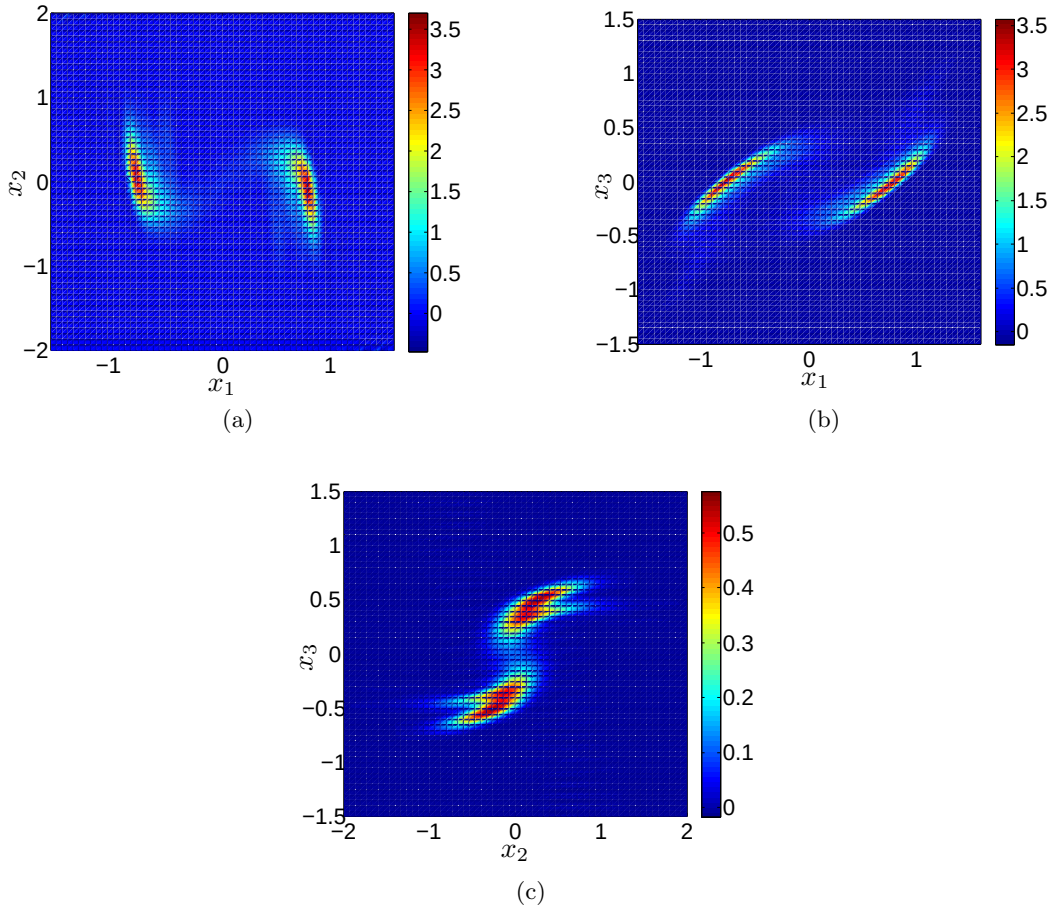

Figure 3.3: Cross-sectional views of the resulting stationary PDF for (a) x_1 and x_2 when $x_3 = 0$, (b) x_1 and x_3 when $x_2 = 0$, and (c) x_2 and x_3 when $x_1 = 0$. Results are obtained for $\delta = 1.5$, $\alpha = 0.5$, $\kappa = 0.65$, $\zeta = 0.01$ and $S_0 = 0.01$.

Fig. 3.4 compares the statistical averages obtained via the FEM to those obtained via a direct numerical integration of the original stochastic differential equations, Equation (2.8). The numerical integration is carried out using Matlab's communication toolbox. Figure 3.4(a) illustrates that the mean displacement obtained using FEM is always zero regardless of the value of δ. This implies that, even when the potential wells are very deep, dynamic trajectories can still escape from a single potential well and, on average, the harvester performs inter-well oscillations with zero mean value about the saddle point. In comparison, results from numerical integration show that the mean displacement starts to

deviate from zero as δ decreases. For the results of the numerical integration to converge to zero, a much longer time span, in the order of days, should be considered as depicted in Fig. 3.5. The figure shows the convergence of the numerical solution to the FEM results for two different integration times with the closer response obtained using an integration time that is ten times the other. The issue of convergence of the numerical solutions becomes even more prevalent when the noise intensity is decreased.

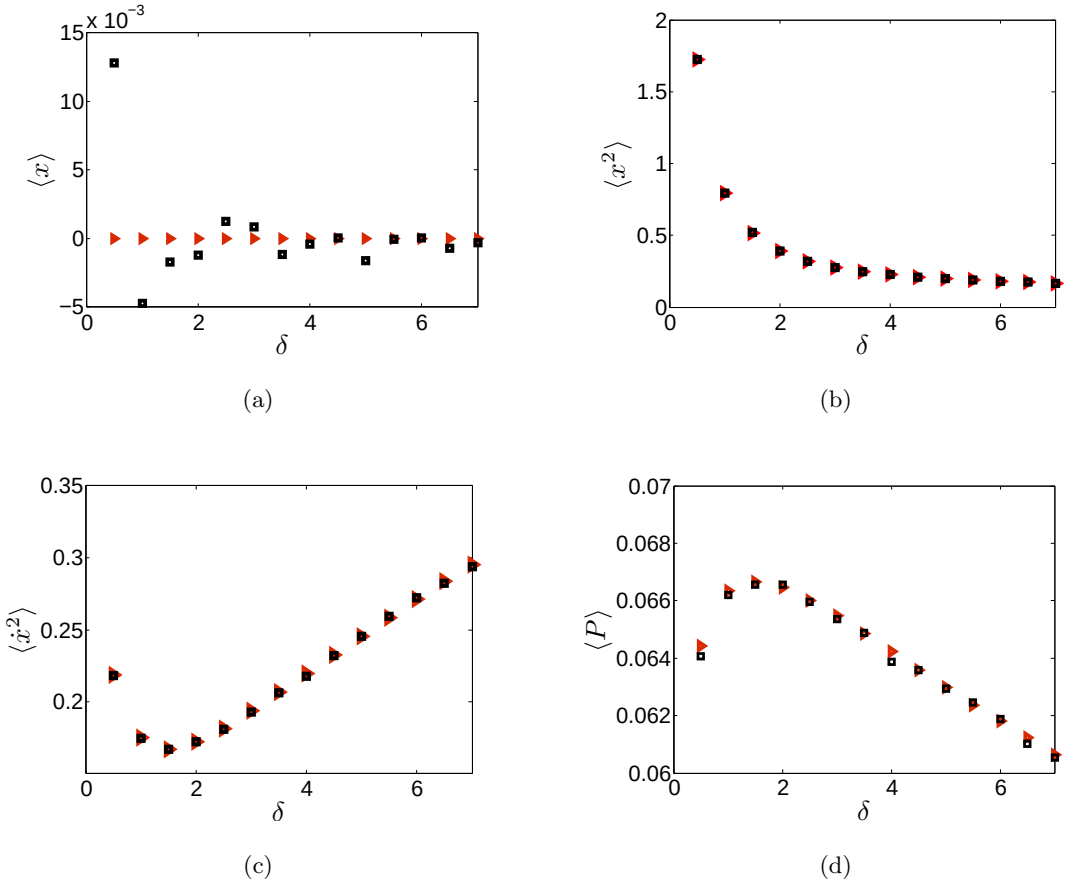

Figure 3.4: Variation of (a) $\langle x \rangle$, (b) $\langle x^2 \rangle$, (c) $\langle \dot{x}^2 \rangle$, and (d) $\langle \mathrm{P} \rangle$ with the nonlinearity δ obtained for $\alpha = 0.5$, $\kappa = 0.65$, $\zeta = 0.01$ and $S_0 = 0.01$. Squares and triangles represent solutions obtained via Numerical Integration and FEM, respectively.

Results from the FEM are further compared to those obtained using SL as shown in Fig. 3.6. It can be clearly seen that none of the solutions obtained using SL predicts

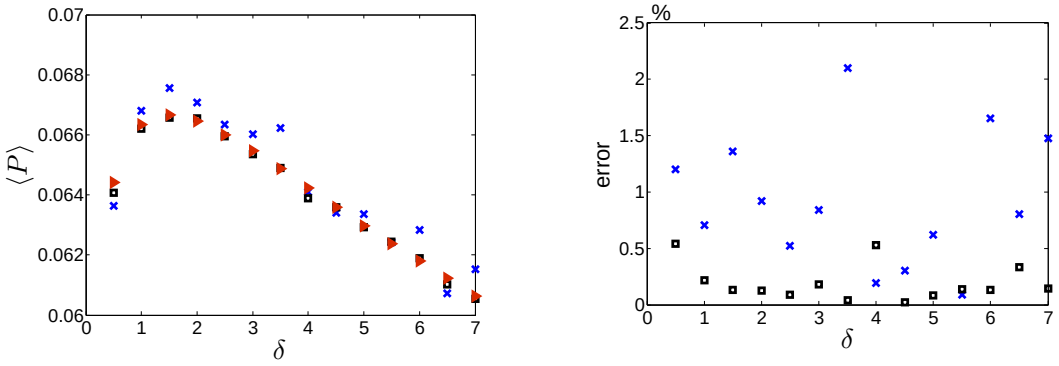

(a) (b)

Figure 3.5: Variation of (a) ⟨P⟩, and (b) percentage error with the nonlinearity δ obtained for $\alpha = 0.5$, $\kappa = 0.65$, $\zeta = 0.01$, and $S_0 = 0.01$. Triangles represent solutions obtained using FEM while the squares and the crosses represent solutions obtained via Numerical Integration. The simulated time for squares is ten times that of the crosses.

the actual response statistics for small values of δ. Only when δ becomes sufficiently large that the solution associated with $\langle x \rangle = 0$ converges to the FE solution. The SL results also reveal that the power does not exhibit an optimal value but continues to decrease as δ increases. As a result, SL can only be used to study the dynamics of the VEH when the potential wells are shallow and closely spaced. In such a scenario, the power always decreases with δ similar to a mono-stable VEH possessing a symmetric potential function [27].

3.4 Influence of The Potential Shape on the Output Power

Since, as discussed in the previous section, SL produces erroneous predictions for the output power especially for small values of δ, numerical simulations that are cross-validated with FE results are used in this section to study the influence of the shape of the potential function on the output power.

First, it should be noted that, when the time constant ratio is very large, the shape of the potential function embedded within δ has very little influence on the output power

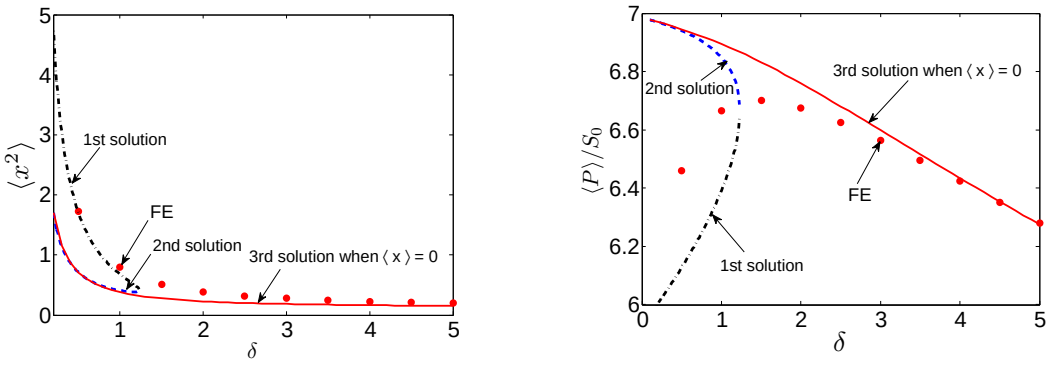

(a) (b)

Figure 3.6: Variation of (a) $\langle x^2 \rangle$ and (b) $\langle \mathrm{P} \rangle$ with nonlinearity δ obtained for $\kappa = 0.65$, $\zeta = 0.01$ and $S_0 = 0.01$ for different α via FE and SL method.

as shown in Fig. 3.7 (a). As such, the study of the influence of the potential shape on the output power becomes irrelevant. When α is large, the electric output, y, becomes directly proportional to the velocity, $\dot{x}$, and loses its direct dependence on the displacement, x, as can be seen in Equation (2.4). This reduces the influence of the shape of the potential function on the output power as has also been proven analytically by Daqaq in [14, 16]. On the other hand, as α decreases, the power exhibits a clear dependence on the shape of the potential function and can also exhibit a maximum at an optimal value of δ.

Fig. 3.7 (a) further illustrates that this optimal value of δ decreases with the time constant ratio and approaches zero as α approaches zero. To explain this behavior, we first discuss the case when α approaches zero. In such a scenario, the electric output becomes directly proportional to the displacement as per Equations (2.4b). As a result, the optimal value of $\langle y^2 \rangle$ approaches the optimal value of $\langle x^2 \rangle$. To find the optimal value of $\langle x^2 \rangle$, we reexamine the FEM results which predict that, for white noise, the mean square value of the displacement takes its maximum value when δ approaches zero; that is, when the potential energy function has a global maximum at $x = 0$. Such results make physical sense, because the mean square displacement approaches infinity when the potential well has one unstable saddle. This conclusion regarding the optimal value of $\langle x^2 \rangle$ holds for any value of α.

Now, back to the case when α is not necessarily close to zero. In this case, δ exhibits an optimal value which is different from zero. To approximate this value analytically, Cottone et al. [13] used an intelligent approach where they balanced the Kramer's inter-well transition rate with the separation distance between the wells to maximize the mean square displacement. Then, using the argument that the optimal value of $\langle y^2 \rangle$ approaches the optimal value of $\langle x^2 \rangle$ for sufficiently small values of α, they obtained $\delta_{opt} = \frac{1}{2\pi S_0 \tau_c}$ where τ_c is the correlation time of the noise. Using this approach for white noise ($\tau_c \to 0$), yields $\delta_{opt} \to 0$ which is quite different from the optimal value obtained using the FEM analysis. As such, Cottone's approach of approximating the optimal value analytically cannot be used to predict the optimal potential shape that maximizes the average power for the white noise case.

It can also be seen in Figs. 3.7 (b) and Fig. 3.8, that the optimal potential shape embedded within δ has a clear dependence on the noise intensity. Results clearly illustrate that δ_{opt} decreases with S_0 meaning that a potential function with deeper and more widely-separated wells is necessary to maximize the average power as the noise intensity increases. If the potential shape is not optimized for a given noise intensity, significant reduction in the output power is expected. For instance, when $S_0 = 0.1$, the mean power drops by around 15% as δ changes from its optimal value of 0.1 to the arbitrary chosen value of $\delta = 1$. Variation of the average power with δ becomes even more prevalent as the noise intensity of the source increases.

Variation of the optimal average power and the associated electrical load embedded within the time constant ratio α with δ are displayed in Fig. 3.9 for a fixed noise intensity. It is evident that the optimal load can result in an optimal time constant ratio α which is not necessarily small. This brings to question the argument raised previously by various researchers which states that α must be small for enhanced energy harvesting using a bi-stable harvester. While reducing α amplifies the influence of the nonlinearity on the output voltage, it does not guarantee optimal performance. This can also be clearly seen by reinspecting Fig. 3.7 (a) and noticing that, while maximum variation of the mean power

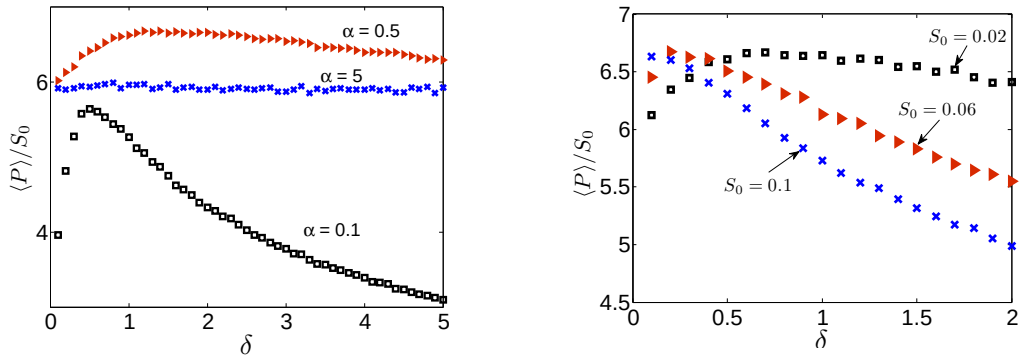

(a) (b)

Figure 3.7: Variation of the average power ⟨P⟩ with the nonlinearity δ for different values of α and S_0 for (a) S_0=0.01 and (b) $\alpha = 0.5$. Results are obtained for $\kappa = 0.65$, and $\zeta = 0.01$.

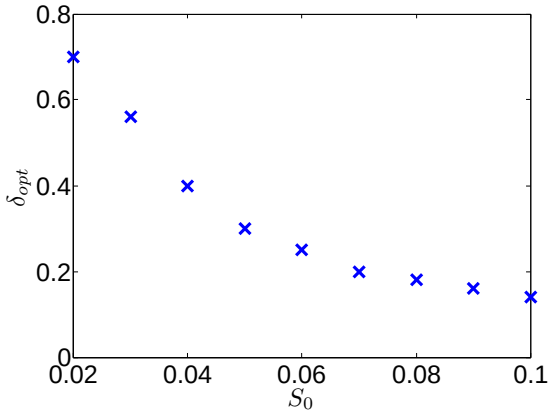

Figure 3.8: Variation of optimal δ with the input variance S_0. Results are obtained for $\kappa = 0.65$, $\zeta = 0.01$ and $\alpha = 0.5$.

with δ occurs for smaller values of $\alpha = 0.1$, the maximum attainable power occurs for an intermediate value of $\alpha = 0.5$.

3.5 Influence of Potential Asymmetry on the Output Power

The design of a perfectly symmetric bi-stable potential function for energy harvesting is a very challenging task. For instance, in buckled-beam type harvesters, structural

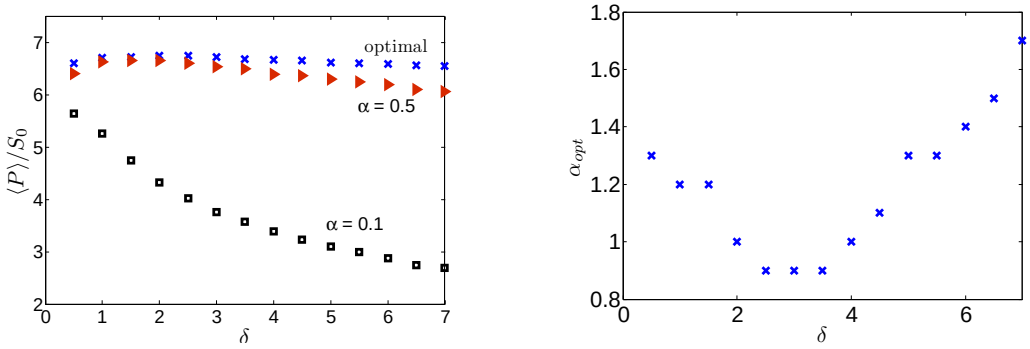

(a) (b)

Figure 3.9: Variation of the optimal average power (a)⟨P⟩ and (b)α with the nonlinearity δ. Results are obtained for $\kappa = 0.65$, $\zeta = 0.01$.

imperfections, initial curvature, added masses, as well as asymmetries in the externally applied magnetic fields can produce asymmetry in the potential function. When the potential function is asymmetric, the harvester's response does not necessarily have zero mean value under white noise excitations. This can significantly influence the harvester's performance and efficacy.

To analyze the influence of potential asymmetry on the average power, we adopt the restoring force in Equation (2.5) which includes a quadratic nonlinearity with coefficient, λ. When λ is greater than $2\sqrt{\delta}$, the potential function switches from being a mono-stable asymmetric potential to a bi-stable asymmetric potential. As shown in Fig. 2.3(a), when $\lambda = 3\sqrt{\delta/2}$, the bi-stable potential recovers its symmetric properties. Increasing λ further causes the potential function to become asymmetric again. The influence of varying λ and δ on the shape of the potential energy function is displayed in Fig. 3.10. The coefficient λ controls the symmetry properties of the potential function while δ controls the depth and separation distance between the wells.

We use the finite element analysis described in section 3.2 to obtain the potential energy function as depicted in Fig. 3.11 which provides a cross-sectional view of the PDF for different sets of variables, $\{x_1, x_2\}$, $\{x_1, x_3\}$, $\{x_2, x_3\}$, respectively, and $\lambda = \sqrt{17\delta/4}$. It

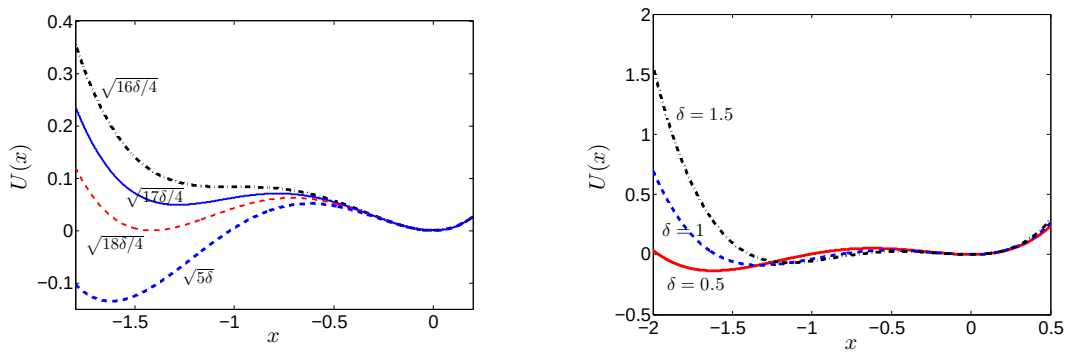

(a) (b)

Figure 3.10: (a) Potential energy function for different values of λ when $\delta = 1$ and (b) Potential energy function for different values of δ when $\lambda = \sqrt{5\delta}$.

is evident that the PDF does not possess symmetric properties with the dynamics clearly having higher probability of being near the deeper potential well as shown in Fig. 3.11(a). A comparison between the FE solution and the numerical integration of the stochastic differential equations is shown in Fig. 3.12 clearly demonstrating an excellent agreement.

Figure 3.13 depicts variation of the mean square displacement and mean power of the harvester with δ for a small noise intensity of $S_0 = 0.01$ and different values of λ. It is evident that the harvester possessing the symmetric potential function provides larger mean power over most of the range considered. The potential energy function with the highest asymmetric properties, $\lambda = \sqrt{5\delta}$, seems to provide the lowest power levels when δ is small, but recovers to provide the largest power level when δ becomes very large. Nevertheless, when designed using the optimal value of δ, the symmetric bi-stable harvester provides more power levels than all other values of λ.

Similar results can be seen when S_0 is increased to the intermediate values of $S_0 = 0.04$ and 0.05 as depicted in Fig. 3.14 with the main difference that the energy harvester with the highly asymmetric potential can now outperform the symmetric one for smaller values of δ. However, when all harvesters are designed to operate using their optimal value of δ, the one with the symmetric potential still provide the maximum average power. When S_0 is

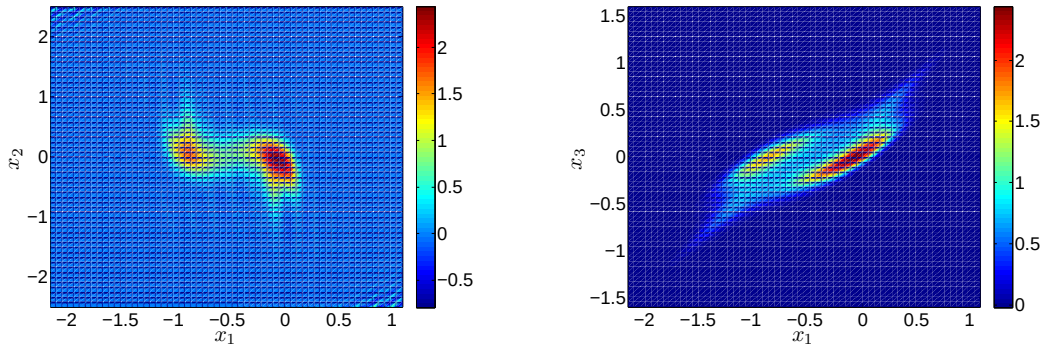

(a)

(b)

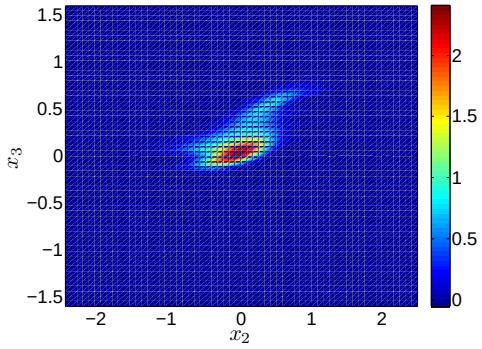

(c)

Figure 3.11: Cross-sectional views of the resulting stationary PDF for (a) x_1 and x_2 when $x_3 = 0$, (b) x_1 and x_3 when $x_2 = 0$,(c) x_2 and x_3 when $x_1 = 0$. Results are obtained for $\delta = 1$, $\lambda = \sqrt{17/4}$, $\kappa = 0.65$, $\zeta = 0.01$, $\alpha = 0.5$ and $S_0 = 0.01$.

increased significantly to 0.5 as depicted in Fig. 3.15, the effect of the potential asymmetry diminishes and the mean power curves converge nicely into one curve.

The effect of potential symmetry and noise intensity can also be seen by inspecting variation of the mean power with λ for different values of S_0 as depicted in Fig. 3.16. It is evident that mean power increases initially and reaches an optimal values which is very close to that associated with the symmetric potential. The power then decreases monotonically with λ clearly illustrating the detrimental influence of potential asymmetries on the output power. Variation of the power is also clearly less prominent as S_0 increases, further

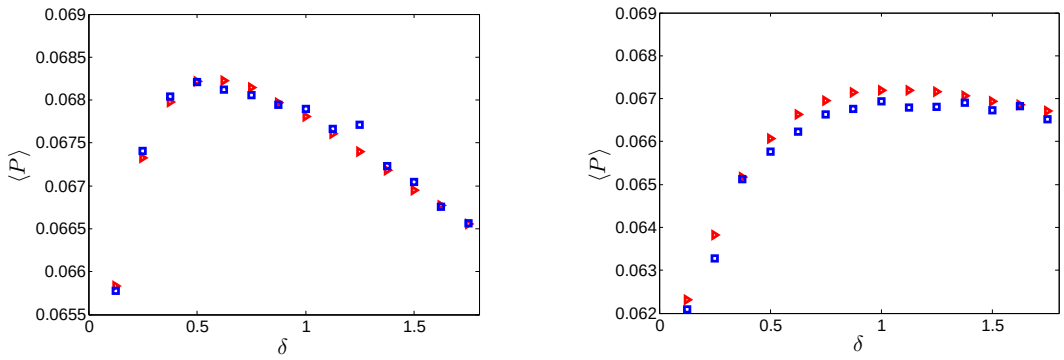

(a) (b)

Figure 3.12: Variation of $\langle P \rangle$ with δ obtained for $\kappa = 0.65$, $\zeta = 0.01$, $\alpha = 0.5$, $S_0 = 0.01$, (a) $\lambda = \sqrt{17\delta/4}$ and (b) $\lambda = \sqrt{5\delta}$. Squares and triangles represent solutions obtained via Numerical Integration and FEM, respectively

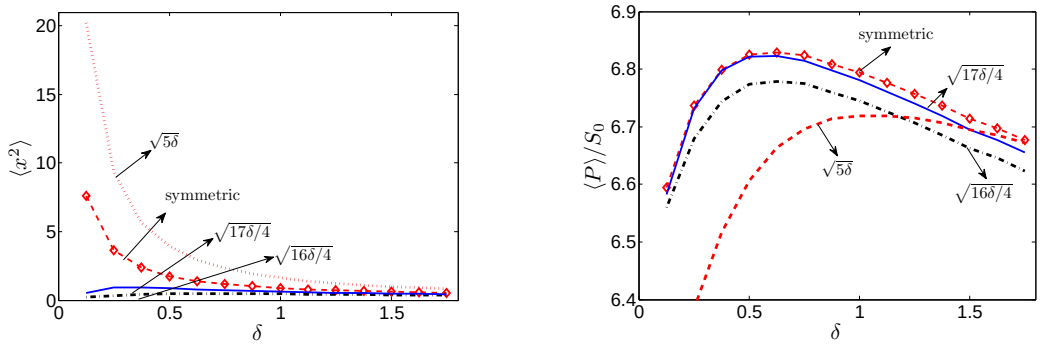

(a) (b)

Figure 3.13: Variation of $\langle x^2 \rangle$ and $\langle P \rangle$ with δ obtained for $\kappa = 0.65$, $\zeta = 0.01$, $\alpha = 0.5$ and $S_0 = 0.01$

highlighting the diminishing influence of potential asymmetry for larger noise intensities.

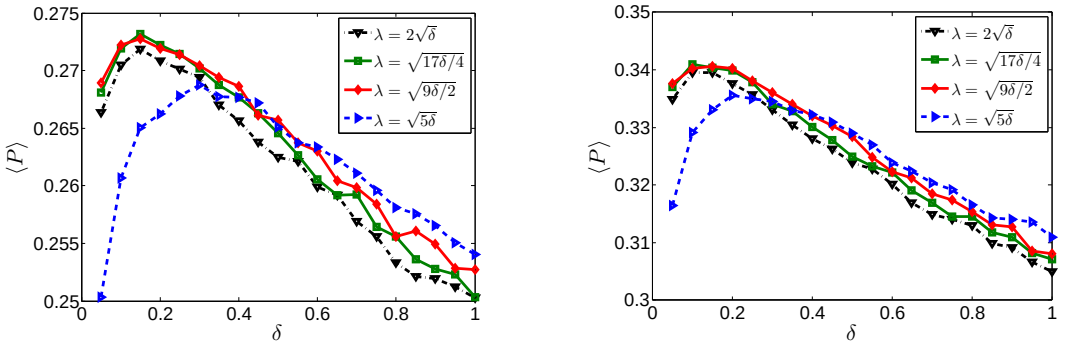

(a) (b)

Figure 3.14: Variation of $\langle P \rangle$ with δ obtained for $\kappa = 0.65$, $\zeta = 0.01$, $\alpha = 0.5$ when (a)$S_0 = 0.04$ and (b)$S_0 = 0.05$

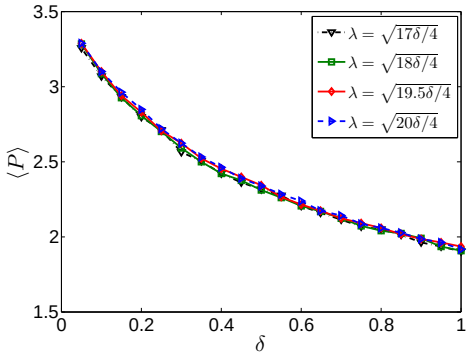

Figure 3.15: Variation of $\langle P \rangle$ with δ obtained for $\kappa = 0.65$, $\zeta = 0.01$, $\alpha = 0.5$, and $S_0 = 0.5$

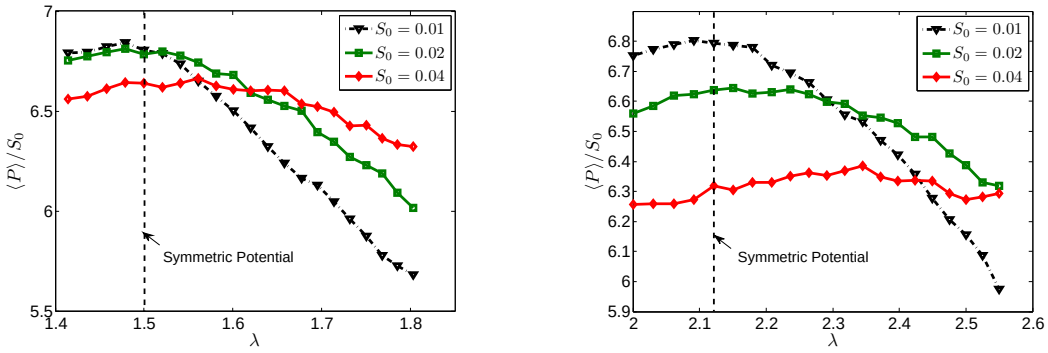

(a) (b)

Figure 3.16: Variation of $\langle P \rangle$ with λ obtained for $\kappa = 0.65$, $\zeta = 0.01$, $\alpha = 0.5$ when (a)$\delta = 0.5$ and (b)$\delta = 1$

Chapter 4

Conclusions

This thesis investigated the influence of stiffness nonlinearities on the performance of energy harvesters subjected to white noise excitations. Both mono-stable and bistable VEHs were considered.

For the mono-stable VEHs, both symmetric and asymmetric nonlinear restoring forces were investigated. It was clearly shown that, the optimal electrical load depends on the nonlinearity especially when the ratio between the period of the mechanical system and the time constant of the harvesting circuit is not large. Mono-stable harvesters with a symmetric potential shape are demonstrated to produce smaller average power levels when compared to the linear VEH with an equivalent stiffness. On the other hand, for VEHs with asymmetric restoring forces, the average power is observed to be larger as compared to a linear device.

Subsequently, the response of a bi-stable energy harvester to white noise excitations is analyzed. To obtain the optimal potential shape which maximizes the mean power for a given noise intensity, statistical linearization, direct numerical integration method, and finite element solution of the Fokker-Plank-Kolmogorov equation were utilized. It was observed that, statistical linearization generates non-unique and erroneous results unless the potential energy function has shallow potential wells. On the other hand, both of the finite element solution and the direct numerical integration provide close predictions for the

mean power regardless of the shape of the potential energy function. However, convergence of the numerical integration approach can be very slow especially when the potential wells are very deep and the noise intensity is small.

Using the solution from finite element analysis, we arrived at the following conclusion:

- The mean power exhibits a maximum value at an optimal potential shape. This optimal shape does not correspond to the shape that maximizes the mean square displacement even when the time constant ratio between the time constants of the mechanical and electrical systems is small. In fact, maximizing the mean square displacement yields a potential shape with a global maximum (unstable potential) regardless of the time constant ratio and noise intensity, whereas maximizing the average power yields a bi-stable potential function which possesses deeper potential wells for larger noise intensities and vise versa.

- Apart from the optimal shape, the average power decreases significantly demonstrating the necessity of characterizing the noise intensity of the vibration source prior to designing a bi-stable harvester for the purpose of harvesting energy from white noise excitations.

- The optimal time constant ratio will not necessarily be small which challenges previous conceptions that a bi-stable harvester provides better output power when the time constant ratio is small. While maximum variation of the mean power with the nonlinearity occurs for smaller values of time constant ratio, this does not necessarily correspond to the optimal performance of the harvester.

- The asymmetry of potential energy function can enhance the power output only when the cubic nonlinearity is large and quadratic nonlinearity can exceed the critical symmetric value. Furthermore, under large white noise excitation, the value of quadratic nonlinearity can decrease, beyond which the asymmetric harvester would outperform the symmetric one.

Having evaluated the influence of stiffness-type nonlinearities on energy harvesting under white noise, further research efforts should investigate other types of nonlinearities e.g., nonlinearities in the harvesting circuit dynamics or in the velocity to enhance the transduction of energy harvesters under random excitations which can be approximated by a white noise process. Other types of excitations that exhibit properties should also be discussed because they provide a better representation of actual environmental excitations.

Bibliography

[1] A. Abdelkefi, A. H. Nayfeh, and M. Hajj. Effects of Nonlinear Piezoelectric Coupling on Energy Harvesters under Direct Excitation. Nonlinear Dynamics, 2011.

[2] A. Abdelkefi, A. H. Nayfeh, and M. Hajj. Global Nonlinear Distributed-parameter Model of Parametrically Excited Piezoelectric Energy Harvesters. Nonlinear Dynamics, 2011.

[3] S. Adhikari, M. I. Friswell, and D. J. Inman. Piezoelectric Energy Harvesting from Broadband Random Vibrations. Smart Materials and Structures, 18, 2009.

[4] K. Baerta, B. Gyselinckxa, T. Torfsa, V. Leonova, F. Yazicioglua, S. Brebelsa, S. Donnaya, J. Vanfleterena, E. Beyna, and C. Van Hoof. Technologies for Highly Miniaturized Autonomous Sensor Newtorks. Microelectronics Journal, 37:1563–1568, 2006.

[5] J. Baker, S. Roundy, and P. Wright. Alternative Geometries for Increasing Power Density in Vibration Energy Scavenging for Wireless Sensors. In Proceedings of the Third International Energy Conversion Conference, pages 959–970, San Francisco, CA, 2005.

[6] D. Barton, S. Burrow, and L. Clare. Energy Harvesting from Vibrations with a Nonlinear Oscillator. In Proceedings of the ASME 2009 International Design Engineering Technical Conference and Computers and Information in Engineering Conference, San Diego, CA, 2009.

[7] D. Barton, S. Burrow, and L. Clare. Energy Harvesting From Vibrations With a Nonlinear Oscillator. Journal of Vibration and Acoustics, 132:0210091, 2010.

[8] W. Bracke, P. Merken, R. Puers, and C. Van Hoof. Generic Architectures and Design Methods for Autonomous Sensors. Sensors and Actuators A, 135:881–888, 2007.

[9] V. Challa, M. Prasad, Y. Shi, and F. Fisher. A Vibration Energy Harvesting Device with Bidirectional Resonance Frequency Tunability. Smart Materials and Structures, 75:1–10, 2008.

[10] H. L. Chau and K. D. Wise. Noise Due to Brownian Motion in Ultrasensitive Solid-State Pressure Sensors. IEEE Transactions on Electron Devices, 34, 1987.

[11] Robert D Cook et al. Concepts and Applications of finite element analysis. Wiley. com, 2007.

[12] F. Cottone, H. Vocca, and L. Gammaitoni. Nonlinear Energy Harvesting. Physical Review Letters, 102:080601–1–080601–4, 2009.

[13] F Cottone, H Vocca, and L Gammaitoni. Nonlinear Energy Harvesting. Physical Review Letters, 102(8):080601, 2009.

[14] M. F. Daqaq. Response of Uni-Modal Duffing Type Harvesters to Random Forced Excitations. Journal of Sound and Vibration, 329:3621–3631, 2010.

[15] M. F. Daqaq. Transduction of a Bistable Inductive Generator Driven by White and Exponentially Correlated Gaussian Noise. Journal of Sound and Vibration, 330:2554–2564, 2011.

[16] M. F. Daqaq. On Intentional Introduction of Stiffness Nonlinearities for Energy Harvesting under White Gaussian Excitations. Nonlinear Dynamics, DOI: 10.1007/s11071-012-0327-0, 2012.

[17] M. F. Daqaq and D. Bode. Exploring the Parametric Amplification Phenomenon for Energy Harvesting. Journal of Systems and Control Engineering, 225:456–466, 2010.

[18] M. F. Daqaq, C. Stabler, T. Seuaciuc-Osorio, and Y. Qaroush. Investigation of Power Harvesting via Parametric Excitations. Journal of Intelligent Material Systems and Structures, 20:545–557, 2009.

[19] N. Elvin and A. Erturk. Advances in Energy Harvesting Methods. Springer, 2013.

[20] A. Erturk, J. Hoffman, and D. J. Inman. A Piezo-Magneto-Elastic Structure for Broadband Vibration Energy Harvesting. Applied Physics Letters, 94:254102, 2009.

[21] M. Ferrari, V. Ferrari, M. Guizzetti, B. Andò, S. Baglio, and C. Trigona. Improved Energy Harvesting from Wideband Vibrations by Nonlinear Piezoelectric Converters. Sensors and Actuators A: Physical, 162(2):425–431, 2010.

[22] L. Gammaitoni, I. Neri, and H. Vocca. Nonlinear Oscillators for Vibration Energy Harvesting. Applied Physics Letters, 94, 2009.

[23] PL Green, K. Worden, K. Atallah, and ND Sims. The Benefits of Duffing-type Nonlinearities and Electrical Optimisation of a Mono-stable Energy Harvester Under White Gaussian Excitations. Journal of Sound and Vibration, 2012.

[24] S. Gregori, Y. Li, H. Li, J. Liu, and F. Maloberti. 2.45 GHz Power and Data Transmission for a Low-Power Autonomous Sensors Platform. ISLPED 04, pages 269–273, 2004.

[25] E. Halvorsen. Energy harvesters driven by broadband random vibrations. Journal of Microelectromechanical Systems, 17(5):1061–1071, 2008.

[26] Einar Halvorsen. Fundamental Issues In Nonlinear Wide-band Vibration Energy Harvesting. arXiv preprint arXiv:1209.3184, 2012.

[27] Q. He and M. F. Daqaq. Load Optimization of a Nonlinear Mono-Stable Duffing-Type Harvester Operating in a White Noise Environment. In Proceedings of the ASME 2013 International Design Engineering Technical Conference and Computers and Information in Engineering Conference, IDETC/CIE 2013, Portland, OR, 2013.

[28] K. Ito. Stochastic Integral. Proceedings of the Imperial Academy, Tokyo, 20:519–524, 1944.

[29] A. H. Jazwinski. Stochastic Processes and Filtering Theory. Academic Press, NY, 1970.

[30] N. A. Khovanova and I. A. Khovanov. The Role of Excitations Statistic and Nonlinearity in Energy Harvesting from Random Impulsive Excitations. Applied Physics Letters, 99(14):144101, 2011.

[31] J. W. Kim, H. Takao, K. Sawada, and M. Ishida. Integrated Inductors for RF Transmitters in CMOS/MEMS Smart Microsensor Systems. Sensors, 7:1387–1398, 2007.

[32] RS Langley. A Finite Element Method for The Statistics of Non-linear Random Vibration. Journal of Sound and Vibration, 101(1):41–54, 1985.

[33] G. Litak, M. Borowiec, M. I. Friswell, and S. Adhikari. Energy Harvesting in A Magnetopiezoelastic System Driven by Random Excitations with Uniform and Gaussian Distributions. Journal of Theoretical and Applied Mechanics, 2011.

[34] G. Litak, M. I. Friswell, and S. Adhikari. Magnetopiezoelastic Energy Harvesting Driven by Random Excitations. Applied Physics Letters, 96(21):214103, 2010.

[35] B. Mann and N. Sims. Energy Harvesting from the Nonlinear Oscillations of Magnetic Levitation. Journal of Sound and Vibrations, 319:515–530, 2008.

[36] B. P. Mann and B. A. Owens. Investigations of A Nonlinear Energy Harvester with A Bistable Potential Well. Journal of Sound and Vibration, 329:1215–1226, 2010.

[37] R. Masana and M. F. Daqaq. Comparing the Performance of A Nonlinear Energy Harvester in Mono- and Bi-Stable Potentials. In Proceedings of the ASME 2011 International Design Engineering Technical Conference and Computers and Information in Engineering Conference, Washington, DC, 2011.

[38] R. Masana and M. F. Daqaq. Electromechanical Modeling and Nonlinear Analysis of Axially-Loaded Energy Harvesters. Journal of Vibration and Acoustics, 133:011007, 2011.

[39] R. Masana and M. F. Daqaq. Performance of a Duffing-type Harvester in a Stochastic Environment. Submitted to Journal of Sound and Vibration, 2013.

[40] C.R. McInnes, D.G. Gorman, and M.P. Cartmell. Enhanced Vibrational Energy Harvesting Using Nonlinear Stochastic Resonance. Journal of Sound and Vibration, 318:655–662, 2008.

[41] F. C. Moon and P. J. Holmes. A Magnetoelastic Strange Attractor. Journal of Sound and Vibration, 65:275, 2009.

[42] I. Neri, F. Travasso, H. Vocca, and L. Gammaitoni. Nonlinear Noise Harvesters for Nanosensors. Nano Communication Networks, 2(4):230–234, 2011.

[43] DS Nguyen, E Halvorsen, GU Jensen, and A Vogl. Fabrication And Characterization of a Wideband MEMS Energy Harvester Utilizing Nonlinear Springs. Journal of Micromechanics and Microengineering, 20(12):125009, 2010.

[44] DS Nguyen, E. Halvorsen, GU Jensen, and A. Vogl. Fabrication and characterization of a wideband MEMS energy harvester utilizing nonlinear springs. Journal of Micromechanics and Microengineering, 20(12):125009, 2010.

[45] J. A. Paradiso and Starner T. Energy Scavenging for Mobile and Wireless Electronics. IEEE Pervasive Computing, 4:18–27, 2005.

[46] D. Quinn, L.Triplett, D. Vakakis, and L. Bergman. Comparing Linear and Essentially Nonlinear Vibration-based Energy Harvesting. Journal of Vibration and Acoustics, 133:011001, 2011.

[47] J. Rastegar, C. Pereira, and H. L. Nguyen. Piezoelectric-based Power Sources for Harvesting Energy from Platforms with Low Frequency Vibrations. In Proceedings of Smart Structures and Materials Conference, SPIE, page 617101, San Diego, CA, 2006.

[48] J.B. Roberts and P.D. Spanos. Random vibration and statistical linearization. Dover Publications, 2003.

[49] S. Roundy. On the Effectiveness of Vibration-based Energy Harvesting. Journal of Intelligent Materials and Structures, 16:809–823, 2005.

[50] S. Roundy and Y. Zhang. Toward Self-Tuning Adaptive Vibration-Based Micro-Generators. In Smart Materials, Nano- and Micro-Smart Systems, Sydney, Australia, 2005.

[51] Gael Sebald, Hiroki Kuwano, Daniel Guyomar, and Benjamin Ducharne. Experimental Duffing oscillator for broadband piezoelectric energy harvesting. Smart Materials and Structures, 20(10):102001, 2011.

[52] T. Seuaciuc-Osorio and M. F. Daqaq. Energy Harvesting under Excitations of Time-varying Frequency. Journal of Sound and Vibration, 329:2497–2515, 2010.

[53] S. M. Shahruz. Design of Mechanical Band-Pass Filters for Energy Scavenging. Journal of Sound and Vibrations, 292:987–998, 2006.

[54] S. M. Shahruz. Limits of Performance of Mechanical Band-Pass Filters Used in Energy Harvesting. Journal of Sound and Vibrations, 294:449–461, 2006.

[55] H. Sodano, D. J. Inman, and G.Park. A Review of Power Harvesting from Vibration Using Piezoelectric Materials. The Shock and Vibration Digest, 36:197–205, 2004.

[56] H. Sodano, D. J. Inman, and G.Park. Generation and Storage of Electricity from Power Harvesting Devices. Journal of Intelligent Material Systems and Structures, 16:67–75, 2005.

[57] S. C. Stanton, C. C. McGehee, and B. P. Mann. Nonlinear Dynamics for Broadband Energy Harvesting: Investigation of a Bistable Piezoelectric Inertial Generator. Physica D: Nonlinear Phenomena, 239:640–653, 2010.

[58] W. Wu, Y. Chen, B. Lee, J. He, and Y. Peng. Tunable Resonant Frequency Power Harvesting Devices. In Proceedings of Smart Structures and Materials Conference, SPIE, page 61690A, San Diego, CA, 2006.

[59] P. Yu, Y. Yuan, and J. Xu. Study of Double Hopf Bifurcation and Chaos for an Oscillator with Time-delayed Feedback. Communications in Nonlinear Science and Numerical Simulation, 7:69, 2002.

[60] S. Zhao and A. Erturk. On the Stochastic Excitation of Monostable And Bistable Electroelastic Power Generators: Relative Advantages and Tradeoffs in a Physical System. Journal of Applied Physics, 102, 2013.